

ARTICLES

Measurement of $\alpha_s(M_Z^2)$ from hadronic event observables at the Z^0 resonance

K. Abe,²⁹ I. Abt,¹⁴ C. J. Ahn,²⁶ T. Akagi,²⁷ W. W. Ash,^{27,*} D. Aston,²⁷ N. Bacchetta,²¹ K. G. Baird,²⁴ C. Baltay,³³ H. R. Band,³² M. B. Barakat,³³ G. Baranko,¹⁰ O. Bardon,¹⁶ T. Barklow,²⁷ A. O. Bazarko,¹¹ R. Ben-David,³³ A. C. Benvenuti,² T. Bienz,²⁷ G. M. Bilei,²² D. Bisello,²¹ G. Blaylock,⁷ J. R. Bogart,²⁷ T. Bolton,¹¹ G. R. Bower,²⁷ J. E. Brau,²⁰ M. Breidenbach,²⁷ W. M. Bugg,²⁸ D. Burke,²⁷ T. H. Burnett,³¹ P. N. Burrows,¹⁶ W. Busza,¹⁶ A. Calcaterra,¹³ D. O. Caldwell,⁶ D. Calloway,²⁷ B. Camanzi,¹² M. Carpinelli,²³ R. Cassell,²⁷ R. Castaldi,^{23,†} A. Castro,²¹ M. Cavalli-Sforza,⁷ E. Church,³¹ H. O. Cohn,²⁸ J. A. Coller,³ V. Cook,³¹ R. Cotton,⁴ R. F. Cowan,¹⁶ D. G. Coyne,⁷ A. D'Oliveira,⁸ C. J. S. Damerell,²⁵ S. Dasu,²⁷ R. De Sangro,¹³ P. De Simone,¹³ R. Dell'Orso,²³ M. Dima,⁹ P. Y. C. Du,²⁸ R. Dubois,²⁷ B. I. Eisenstein,¹⁴ R. Elia,²⁷ D. Falcaai,²² C. Fan,¹⁰ M. J. Fero,¹⁶ R. Frey,²⁰ K. Furuno,²⁰ T. Gillman,²⁵ G. Gladding,¹⁴ S. Gonzalez,¹⁶ G. D. Hallewell,²⁷ E. L. Hart,²⁸ Y. Hasegawa,²⁹ S. Hedges,⁴ S. S. Hertzbach,¹⁷ M. D. Hildreth,²⁷ J. Huber,²⁰ M. E. Huffer,²⁷ E. W. Hughes,²⁷ H. Hwang,²⁰ Y. Iwasaki,²⁹ P. Jacques,²⁴ J. Jaros,²⁷ A. S. Johnson,³ J. R. Johnson,³² R. A. Johnson,⁸ T. Junk,²⁷ R. Kajikawa,¹⁹ M. Kalkar,³² I. Karliner,¹⁴ H. Kawahara,²⁷ H. W. Kendall,¹⁶ Y. Kim,²⁶ M. E. King,²⁷ R. King,²⁷ R. R. Kofler,¹⁷ N. M. Krishna,¹⁰ R. S. Kroeger,¹⁸ J. F. Labs,²⁷ M. Langston,²⁰ A. Lath,¹⁶ J. A. Lauber,¹⁰ D. W. G. Leith,²⁷ X. Liu,⁷ M. Loreti,²¹ A. Lu,⁶ H. L. Lynch,²⁷ J. Ma,³¹ G. Mancinelli,²² S. Manly,³³ G. Mantovani,²² T. W. Markiewicz,²⁷ T. Maruyama,²⁷ R. Massetti,²² H. Masuda,²⁷ E. Mazzucato,¹² A. K. McKemey,⁴ B. T. Meadows,⁸ R. Messner,²⁷ P. M. Mockett,³¹ K. C. Moffeit,²⁷ B. Mours,²⁷ G. Müller,²⁷ D. Muller,²⁷ T. Nagamine,²⁷ U. Nauenberg,¹⁰ H. Neal,²⁷ M. Nussbaum,⁸ Y. Ohnishi,¹⁹ L. S. Osborne,¹⁶ R. S. Panvini,³⁰ H. Park,²⁰ T. J. Pavel,²⁷ I. Peruzzi,^{13,‡} L. Pescara,²¹ M. Piccolo,¹³ L. Piemontese,¹² E. Pieroni,²³ K. T. Pitts,²⁰ R. J. Plano,²⁴ R. Prepost,³² C. Y. Prescott,²⁷ G. D. Punkar,²⁷ J. Quigley,¹⁶ B. N. Ratcliff,²⁷ T. W. Reeves,³⁰ P. E. Rensing,²⁷ L. S. Rochester,²⁷ J. E. Rothberg,³¹ P. C. Rowson,¹¹ J. J. Russell,²⁷ O. H. Saxton,²⁷ T. Schalk,⁷ R. H. Schindler,²⁷ U. Schneekloth,¹⁶ B. A. Schumm,¹⁵ A. Seiden,⁷ S. Sen,³³ V. V. Serbo,³² M. H. Shaevitz,¹¹ J. T. Shank,³ G. Shapiro,¹⁵ S. L. Shapiro,²⁷ D. J. Sherden,²⁷ C. Simopoulos,²⁷ N. B. Sinev,²⁰ S. R. Smith,²⁷ J. A. Snyder,³³ P. Stamer,²⁴ H. Steiner,¹⁵ R. Steiner,¹ M. G. Strauss,¹⁷ D. Su,²⁷ F. Suekane,²⁹ A. Sugiyama,¹⁹ S. Suzuki,¹⁹ M. Swartz,²⁷ A. Szumilo,³¹ T. Takahashi,²⁷ F. E. Taylor,¹⁶ E. Torrence,¹⁶ J. D. Turk,³³ T. Usher,²⁷ J. Va'vra,²⁷ C. Vannini,²³ E. Vella,²⁷ J. P. Venuti,³⁰ P. G. Verdini,²³ S. R. Wagner,²⁷ A. P. Waite,²⁷ S. J. Watts,⁴ A. W. Weidemann,²⁸ J. S. Whitaker,³ S. L. White,²⁸ F. J. Wickens,²⁵ D. A. Williams,⁷ D. C. Williams,¹⁶ S. H. Williams,²⁷ S. Willocq,³³ R. J. Wilson,⁹ W. J. Wisniewski,⁵ M. Woods,²⁷ G. B. Word,²⁴ J. Wyss,²¹ R. K. Yamamoto,¹⁶ J. M. Yamartino,¹⁶ X. Yang,²⁰ S. J. Yellin,⁶ C. C. Young,²⁷ H. Yuta,²⁹ G. Zapalac,³² R. W. Zdarko,²⁷ C. Zeitlin,²⁰ and J. Zhou²⁰

(SLD Collaboration)

¹Adelphi University, Garden City, New York 11530²INFN Sezione di Bologna, I-40126 Bologna, Italy³Boston University, Boston, Massachusetts 02215⁴Brunel University, Uxbridge, Middlesex UB8 3PH, United Kingdom⁵California Institute of Technology, Pasadena, California 91125⁶University of California at Santa Barbara, Santa Barbara, California 93106⁷University of California at Santa Cruz, Santa Cruz, California 95064⁸University of Cincinnati, Cincinnati, Ohio 45221⁹Colorado State University, Fort Collins, Colorado 80523¹⁰University of Colorado, Boulder, Colorado 80309¹¹Columbia University, New York, New York, 10027¹²INFN Sezione di Ferrara and Università di Ferrara, I-44100 Ferrara, Italy¹³INFN Laboratori Nazionali di Frascati, I-00044 Frascati, Italy¹⁴University of Illinois, Urbana, Illinois 61801¹⁵Lawrence Berkeley Laboratory, University of California, Berkeley, California 94720¹⁶Massachusetts Institute of Technology, Cambridge, Massachusetts 02139

*Deceased.

†Also at the Università di Genova.

‡Also at the Università di Perugia.

¹⁷ *University of Massachusetts, Amherst, Massachusetts 01003*

¹⁸ *University of Mississippi, University, Mississippi 38677*

¹⁹ *Nagoya University, Chikusa-ku, Nagoya 464 Japan*

²⁰ *University of Oregon, Eugene, Oregon 97403*

²¹ *INFN Sezione di Padova and Università di Padova, I-35100 Padova, Italy*

²² *INFN Sezione di Perugia and Università di Perugia, I-06100 Perugia, Italy*

²³ *INFN Sezione di Pisa and Università di Pisa, I-56100 Pisa, Italy*

²⁴ *Rutgers University, Piscataway, New Jersey 08855*

²⁵ *Rutherford Appleton Laboratory, Chilton, Didcot, Oxon OX11 0QX United Kingdom*

²⁶ *Sogang University, Seoul, Korea*

²⁷ *Stanford Linear Accelerator Center, Stanford University, Stanford, California 94309*

²⁸ *University of Tennessee, Knoxville, Tennessee 37996*

²⁹ *Tohoku University, Sendai 980, Japan*

³⁰ *Vanderbilt University, Nashville, Tennessee 37235*

³¹ *University of Washington, Seattle, Washington 98195*

³² *University of Wisconsin, Madison, Wisconsin 53706*

³³ *Yale University, New Haven, Connecticut 06511*

(Received 19 September 1994)

The strong coupling $\alpha_s(M_Z^2)$ has been measured using hadronic decays of Z^0 bosons collected by the SLD experiment at SLAC. The data were compared with QCD predictions both at fixed order $O(\alpha_s^2)$ and including resummed analytic formulas based on the next-to-leading logarithmic approximation. In this comprehensive analysis we studied event shapes, jet rates, particle correlations, and angular energy flow, and checked the consistency between $\alpha_s(M_Z^2)$ values extracted from these different measures. Combining all results we obtain $\alpha_s(M_Z^2) = 0.1200 \pm 0.0025(\text{expt}) \pm 0.0078(\text{theor})$, where the dominant uncertainty is from uncalculated higher order contributions.

PACS number(s): 12.38.Qk, 13.38.Dg, 13.87.-a

I. INTRODUCTION

Achieving precision tests of the standard model of elementary particle interactions is one of the key aims of experimental high-energy physics experiments. Some measurements in the electroweak sector have reached a precision of better than 1% [1]. However, measurements of strong interactions, and hence tests of the theory of quantum chromodynamics (QCD) [2], have not yet achieved the same level of precision. This is largely due to the difficulty of performing QCD calculations, both at high order in perturbation theory and in the nonperturbative regime, where effects due to the hadronization process are important. QCD is a theory with only one free parameter, the strong coupling α_s , which can be written in terms of a scale parameter $\Lambda_{\overline{\text{MS}}}$, where $\overline{\text{MS}}$ denotes the modified minimal subtraction scheme. All tests of QCD can therefore be reduced to a comparison of measurements of α_s , either in different hard processes, such as hadron-hadron collisions or e^+e^- annihilations, or at different energy scales Q . In this paper we present measurements of α_s in hadronic decays of Z^0 bosons produced by e^+e^- annihilations at the SLAC Linear Collider (SLC) and recorded in the SLC Large Detector.

Complications arise in making accurate QCD predictions. In practice, because of the large number of Feynman diagrams involved, QCD calculations are only possible with present techniques to low order in perturbation theory. Perturbative calculations are performed within a particular *renormalization scheme* [3], which also defines the strong coupling. Translation between different schemes is possible, without changing the final predictions, by appropriate redefinition of α_s and of the *renor-*

malization scale [4]. This leads to a *scheme dependence* of α_s , which can be alleviated in practice by choosing one particular scheme as a standard and translating all α_s measurements to it. The $\overline{\text{MS}}$ scheme [3] is presently used widely as this standard. An additional complication is the truncation of the perturbative series at finite order, which yields a residual dependence on the renormalization scale, often denoted by μ or equivalently by $f = \mu^2/Q^2$, which then becomes an arbitrary unphysical parameter.

In our previous studies of jet rates [5] and energy-energy correlations [6] it was shown that the dominant uncertainty in $\alpha_s(M_Z^2)$ measurements arises from this *renormalization scale ambiguity*. Given that infinite-order perturbative QCD calculations would be independent of μ , the scale uncertainty inherent in α_s measurements is a reflection of the neglected higher-order terms.

Distributions of observables in the process $e^+e^- \rightarrow$ hadrons have been calculated exactly up to $O(\alpha_s^2)$ in QCD perturbation theory [7]. One expects *a priori* that the size of the uncalculated $O(\alpha_s^3)$ and higher-order terms will in general be different for each observable, and hence that the scale dependence of the α_s values measured using different observables will also be different. In order to make a realistic determination of α_s and its associated theoretical uncertainty using $O(\alpha_s^2)$ calculations it is therefore advantageous to employ as many different observables as possible. Our previous measurements of $\alpha_s(M_Z^2)$ were based on extensive studies of jet rates [8] and energy-energy correlations and their asymmetry [9], using approximately 10 000 hadronic Z^0 decays collected by the SLD experiment in 1992. In this comprehensive analysis we have used the combined 1992 and 1993 data samples, comprising approximately 60 000 events,

to make an improved determination of $\alpha_s(M_Z^2)$ using 15 observables presently calculated up to $O(\alpha_s^2)$ in perturbative QCD.

In addition, for 6 of these 15 observables, improved calculations can be formulated incorporating the resummation [10–15] of leading and next-to-leading logarithms matched to the $O(\alpha_s^2)$ results; these matched calculations are expected *a priori* both to describe the data in a larger region of phase space than the fixed-order results, and to yield a reduced dependence of α_s on the renormalization scale. We have employed the matched calculations for all six observables to determine $\alpha_s(M_Z^2)$, and have studied the uncertainties involved in the matching procedure. We have compared our results with our previous measurements and with similar measurements from the CERN e^+e^- collider LEP.

We describe the detector and the event trigger and selection criteria applied to the data in Sec. II. In Sec. III, we define the observables used to determine $\alpha_s(M_Z^2)$ in this analysis. The QCD predictions are discussed in Sec. IV. The analysis of the data is described in Sec. V, and a summary and conclusions are presented in Sec. VI.

II. APPARATUS AND HADRONIC EVENT SELECTION

The e^+e^- annihilation events produced at the Z^0 resonance by the SLAC Linear Collider (SLC) have been recorded using the SLC Large Detector (SLD). A general description of the SLD can be found elsewhere [16]. Charged tracks are measured in the central drift chamber (CDC) and in the vertex detector (VXD) [17]. Momentum measurement is provided by a uniform axial magnetic field of 0.6 T. Particle energies are measured in the liquid-argon calorimeter (LAC) [18], which contains both electromagnetic and hadronic sections, and in the warm iron calorimeter [19].

Three triggers were used for hadronic events. In the 1993 (1992) runs the first required a total LAC electromagnetic energy greater than 12 GeV (8 GeV), the second required at least two well-separated tracks in the CDC, and the third required at least 4 GeV (8 GeV) in the LAC and one track in the CDC. A selection of hadronic events was then made by two independent methods, one based on the topology of energy depositions in the calorimeters, the other on the number and topology of charged tracks measured in the CDC.

The analysis presented here used the charged tracks measured in the CDC and VXD. A set of cuts was applied to the data to select well-measured tracks and events well contained within the detector acceptance. The charged tracks were required to have (i) a closest approach transverse to the beam axis within 5 cm, and within 10 cm along the axis from the measured interaction point, (ii) a polar angle θ with respect to the beam axis within $|\cos\theta| < 0.80$, and (iii) a momentum transverse to the beam axis, $p_\perp > 0.15$ GeV/ c . Events were required to have (i) a minimum of five such tracks, (ii) a thrust axis [20] direction within $|\cos\theta_T| < 0.71$, and (iii) a total visible energy E_{vis} of at least 20 GeV, which was cal-

culated from the selected tracks assigned the charged pion mass. From our 1992 and 1993 data samples 37 226 events passed these cuts. The efficiency for selecting hadronic events satisfying the $|\cos\theta_T|$ cut was estimated to be above 96%. The background in the selected event sample was estimated to be $0.3 \pm 0.1\%$, dominated by $Z^0 \rightarrow \tau^+\tau^-$ events. Distributions of single-particle and event topology observables in the selected events were found to be well described by Monte Carlo models of hadronic Z^0 decays [21,22] combined with a simulation of the SLD.

III. DEFINITION OF THE OBSERVABLES

In this section we present the definitions of the quantities used in our measurement of $\alpha_s(M_Z^2)$. We used observables for which complete $O(\alpha_s^2)$ perturbative QCD calculations exist. These include six event shapes, jet rates defined by six schemes, two particle correlations, and an angular energy flow.

A. Event shapes

Various inclusive observables have been proposed to describe the shapes of hadronic events in e^+e^- annihilations. We considered those observables which are collinear and infrared safe, and which can hence be calculated in perturbative QCD.

Thrust T is defined by [20]

$$T = \max \frac{\sum_i |\mathbf{p}_i \cdot \mathbf{n}_T|}{\sum_i |\mathbf{p}_i|}, \quad (1)$$

where \mathbf{p}_i is the momentum vector of particle i , and \mathbf{n}_T is the thrust axis to be determined. We define $\tau \equiv 1 - T$. For back-to-back two-parton final states τ is zero, while $0 \leq \tau \leq \frac{1}{3}$ for planar three-parton final states. Spherical events have $\tau = \frac{1}{2}$. An axis \mathbf{n}_{maj} can be found to maximize the momentum sum transverse to \mathbf{n}_T . Finally, an axis \mathbf{n}_{min} is defined to be perpendicular to the two axes \mathbf{n}_T and \mathbf{n}_{maj} . The variables thrust major T_{maj} and thrust minor T_{min} are obtained by replacing \mathbf{n}_T in Eq. (1) by \mathbf{n}_{maj} or \mathbf{n}_{min} , respectively. The oblateness O is then defined by [23]

$$O = T_{\text{maj}} - T_{\text{min}}. \quad (2)$$

The value of O is zero for collinear or cylindrically symmetric final states, and extends from zero to $1/\sqrt{3}$ for three-parton final states.

The C parameter is derived from the eigenvalues of the infrared-safe momentum tensor [24]:

$$\theta_{\rho\sigma} = \frac{\sum_i p_i^\rho p_i^\sigma / |\mathbf{p}_i|}{\sum_i |\mathbf{p}_i|}, \quad (3)$$

where p_i^ρ is the ρ th component of the three momentum of particle i , and i runs over all the final-state particles. The tensor $\theta_{\rho\sigma}$ is normalized to have unit trace, and the

C parameter is defined by

$$C = 3(\lambda_1\lambda_2 + \lambda_2\lambda_3 + \lambda_3\lambda_1), \quad (4)$$

where λ_i ($i = 1, 2, 3$) are the eigenvalues of the tensor $\theta_{\rho\sigma}$. For back-to-back two-parton final states C is zero, while for planar three-parton final states $0 \leq C \leq \frac{2}{3}$. For spherical events $C = 1$.

Events can be divided into two hemispheres, a and b , by a plane perpendicular to the thrust axis \mathbf{n}_T . The heavy jet mass M_H is then defined as [25]

$$M_H = \max(M_a, M_b), \quad (5)$$

where M_a and M_b are the invariant masses of the two hemispheres. Here we define the normalized quantity

$$\rho \equiv \frac{M_H^2}{E_{\text{vis}}^2}, \quad (6)$$

where E_{vis} is the total visible energy measured in hadronic events. To first order in perturbative QCD, and for massless partons, the heavy jet mass and thrust are related by $\tau = \rho$ [7].

Jet broadening measures have been proposed in Ref. [26]. In each hemisphere a, b ,

$$B_{a,b} = \frac{\sum_{i \in a,b} |\mathbf{p}_i \times \mathbf{n}_T|}{2 \sum_i |\mathbf{p}_i|} \quad (7)$$

is calculated. The total jet broadening B_T and wide jet broadening B_W are defined by

$$B_T = B_a + B_b \quad \text{and} \quad B_W = \max(B_a, B_b), \quad (8)$$

respectively. Both B_T and B_W are identically zero in two-parton final states and are sensitive to the transverse structure of jets. To first order in perturbative QCD $B_T = B_W = \frac{1}{2}O$.

B. Jet rates

Another useful method of classifying the structure of hadronic final states is in terms of jets. Jets may be reconstructed using iterative clustering algorithms [8] in which a measure y_{ij} , such as scaled invariant mass, is calculated for all pairs of particles i and j , and the pair with the smallest y_{ij} is combined into a single particle. This procedure is repeated until all pairs have y_{ij} exceeding a value y_{cut} , and the jet multiplicity of the event is defined as the number of particles remaining. The n -jet rate $R_n(y_{\text{cut}})$ is the fraction of events classified as n -jet, and the differential two-jet rate is defined as [27]

$$D_2(y_{\text{cut}}) \equiv \frac{R_2(y_{\text{cut}}) - R_2(y_{\text{cut}} - \Delta y_{\text{cut}})}{\Delta y_{\text{cut}}}. \quad (9)$$

In contrast with R_n , each event contributes to D_2 at only one y_{cut} value.

Several schemes have been proposed comprising different y_{ij} definitions and recombination procedures. We

have applied the E , $E0$, P , and $P0$ variations of the JADE algorithm [28] as well as the Durham (D) and Geneva (G) schemes [8]. The six definitions of the jet resolution parameter y_{ij} and recombination procedure are given below.

In the E scheme y_{ij} is defined as the square of the invariant mass of the pair of particles i and j scaled by the visible energy in the event,

$$y_{ij} = \frac{(p_i + p_j)^2}{E_{\text{vis}}^2}, \quad (10)$$

with the recombination performed as

$$p_k = p_i + p_j, \quad (11)$$

where p_i and p_j are the four-momenta of the particles, and pion masses are assumed in calculating particle energies. Energy and momentum are explicitly conserved in this scheme.

The $E0$, P , and $P0$ schemes are variations of the E scheme. In the $E0$ scheme y_{ij} is defined by Eq. (10), while the recombination is defined by

$$E_k = E_i + E_j, \quad (12)$$

$$\mathbf{p}_k = \frac{E_k}{|\mathbf{p}_i + \mathbf{p}_j|} (\mathbf{p}_i + \mathbf{p}_j), \quad (13)$$

where E_i and E_j are the energies and \mathbf{p}_i and \mathbf{p}_j are the three-momenta of the particles. The three-momentum \mathbf{p}_k is rescaled so that particle k has zero invariant mass. This scheme does not conserve the total momentum sum of an event.

In the P scheme y_{ij} is defined by Eq. (10) and the recombination is defined by

$$\mathbf{p}_k = \mathbf{p}_i + \mathbf{p}_j, \quad (14)$$

$$E_k = |\mathbf{p}_k|. \quad (15)$$

This scheme conserves the total momentum of an event, but does not conserve the total energy.

The $P0$ scheme is similar to the P scheme, but the total energy E_{vis} in Eq. (10) is recalculated at each iteration according to

$$E_{\text{vis}} = \sum_k E_k. \quad (16)$$

In the D scheme,

$$y_{ij} = \frac{2\min(E_i^2, E_j^2)(1 - \cos \theta_{ij})}{E_{\text{vis}}^2}, \quad (17)$$

where θ_{ij} is the angle between the pair of particles i and j . The recombination is defined by Eq. (11). With the D scheme a soft particle will be combined with another soft particle, instead of being combined with a high-energy particle, only if the angle it makes with the other soft particle is smaller than the angle that it makes with the high-energy particle.

The definition of y_{ij} for the G scheme is

$$y_{ij} = \frac{8E_i E_j (1 - \cos \theta_{ij})}{9(E_i + E_j)^2}, \quad (18)$$

and the recombination is defined by Eq. (11). In this scheme soft particles are combined as in the D scheme. In addition, y_{ij} depends only on the energy of the particles to be combined, and not on the E_{vis} of the event.

C. Particle correlations

Hadronic event observables can also be classified in terms of inclusive two-particle correlations. The energy-energy correlation (EEC) [9] is the normalized energy-weighted cross section defined in terms of the angle χ_{ij} between two particles i and j in an event:

$$\text{EEC}(\chi) \equiv \frac{1}{N_{\text{events}} \Delta\chi} \sum_{\text{events}} \int_{\chi - \Delta\chi/2}^{\chi + \Delta\chi/2} \sum_{ij} \frac{E_i E_j}{E_{\text{vis}}^2} \delta(\chi' - \chi_{ij}) d\chi', \quad (19)$$

where χ is an opening angle to be studied for the correlations; $\Delta\chi$ is the angular bin width; and E_i and E_j are the energies of particles i and j . The angle χ is taken from $\chi = 0^\circ$ to 180° . The shape of the EEC in the central region, $\chi \sim 90^\circ$, is determined by hard gluon emission. Hadronization contributions are expected to be large in the collinear and back-to-back regions, $\chi \sim 0^\circ$ and 180° , respectively. The asymmetry of the EEC (AEEC) is defined as $\text{AEEC}(\chi) = \text{EEC}(180^\circ - \chi) - \text{EEC}(\chi)$.

D. Angular energy flow

Another procedure, related to the angle of particle emission, is to integrate the energy within a conical shell of opening angle χ about the thrust axis. The jet cone energy fraction (JCEF) is defined [29] as

$$\text{JCEF}(\chi) = \frac{1}{N_{\text{events}} \Delta\chi} \sum_{\text{events}} \int_{\chi - \Delta\chi/2}^{\chi + \Delta\chi/2} \sum_i \frac{E_i}{E_{\text{vis}}} \delta(\chi' - \chi_i) d\chi', \quad (20)$$

where

$$\chi_i = \arccos \left(\frac{\mathbf{p}_i \cdot \mathbf{n}_T}{|\mathbf{p}_i|} \right) \quad (21)$$

is the opening angle between a particle and the thrust axis vector, \mathbf{n}_T , whose direction is defined to point from the heavy jet mass hemisphere to the light jet mass hemisphere, and $0^\circ \leq \chi \leq 180^\circ$. Hard gluon emissions contribute to the region corresponding to the heavy jet mass hemisphere, $90^\circ \leq \chi \leq 180^\circ$.

IV. QCD PREDICTIONS

The QCD predictions up to $O(\alpha_s^2)$ for all observables defined in Sec. III have the general form

$$\frac{1}{\sigma_t} \frac{d\sigma(y)}{dy} = A(y) \tilde{\alpha}_s + [B(y) + A(y) 2\pi b_0 \ln f] \tilde{\alpha}_s^2, \quad (22)$$

where y is the observable in question; σ_t is the total hadronic cross section; $\tilde{\alpha}_s = \alpha_s/2\pi$; $f = \mu^2/s$; $b_0 = (33 - 2n_f)/(12\pi)$; and n_f is the number of active quark flavors; $n_f = 5$ at $\sqrt{s} = M_Z$. We have computed the coefficients $A(y)$ and $B(y)$ using the `EVENT` program, which was developed by Kunszt and Nason [7]. It should be noted that a dependence on the QCD renormalization scale enters explicitly in the second-order term in Eq. (22).

It has been found recently [10–15] that several observables, namely, τ , ρ , B_T , B_W , D_2 (D scheme), and EEC,

can be resummed, that is, leading and next-to-leading logarithmic terms can be calculated to all orders in α_s using an exponentiation technique. This procedure is expected *a priori* to yield formulas which are less dependent on the renormalization scale. Using $L \equiv \ln(1/y)$, the fraction $R(y, \alpha_s)$ can then be written in the general form

$$R(y, \alpha_s) \equiv \frac{1}{\sigma_t} \int_0^y \frac{d\sigma}{dy} dy = C(\alpha_s) \exp\{\Sigma(\alpha_s, L)\} + F(y, \alpha_s), \quad (23)$$

where

$$C(\alpha_s) = 1 + \sum_{n=1}^{\infty} C_n \tilde{\alpha}_s^n, \quad (24)$$

$$\Sigma(\alpha_s, L) = \sum_{n=1}^{\infty} \tilde{\alpha}_s^n \sum_{m=1}^{n+1} G_{nm} L^m, \quad (25)$$

$$F(y, \alpha_s) = \sum_{n=1}^{\infty} F_n(y) \tilde{\alpha}_s^n. \quad (26)$$

The factor Σ to be exponentiated can be written

$$\Sigma(\alpha_s, L) = L f_{\text{LL}}(\alpha_s L) + f_{\text{NLL}}(\alpha_s L) + O\left(\frac{1}{L}(\alpha_s L)^n\right), \quad (27)$$

where $f_{\text{LL}}(\alpha_s L)$ and $f_{\text{NLL}}(\alpha_s L)$ are the leading and next-to-leading logarithms. The functions f_{LL} and f_{NLL} depend only on the product $\alpha_s L$ and are given in

Refs. [10–15]. The resummed calculations are thus given by an approximate expression for $R(y, \alpha_s)$ in the form

$$R^{\text{resum}}(y, \alpha_s) = (1 + C_1 \tilde{\alpha}_s + C_2 \tilde{\alpha}_s^2) \exp\{\Sigma^{\text{resum}}(\alpha_s, L)\}, \quad (28)$$

where

$$\Sigma^{\text{resum}}(\alpha_s, L) = Lf_{\text{LL}}(\alpha_s L) + f_{\text{NLL}}(\alpha_s L). \quad (29)$$

Whereas the leading logarithmic (Lf_{LL}) and next-to-leading logarithmic (f_{NLL}) terms in Σ have been calculated, the subleading terms in Eq. (27) have not been completely computed. However, some subleading terms included in Σ [Eq. (25)], as well as C and F , are included in the $O(\alpha_s^2)$ calculation. In order to make reliable predictions, including hard gluon emission, with the resummed calculations it is necessary to combine them with the second-order calculations, taking overlapping terms into account. This procedure is called *matching*, and four matching schemes have been proposed in the literature.

The $O(\alpha_s^2)$ QCD formula [Eq. (22)] can also be cast

into the integrated form

$$R^{O(\alpha_s^2)}(y, \alpha_s) = 1 + \mathcal{A}(y)\tilde{\alpha}_s + \mathcal{B}(y)\tilde{\alpha}_s^2, \quad (30)$$

where $\mathcal{A}(y)$ and $\mathcal{B}(y)$ are the cumulative forms of $A(y)$ and $B(y)$ in Eq. (22). Taking the logarithm of the resummed formula [Eq. (28)] and the $O(\alpha_s^2)$ formula [Eq. (30)],

$$\ln R^{\text{resum}}(y, \alpha_s) = \Sigma^{\text{resum}}(\alpha_s, L) + C_1 \tilde{\alpha}_s + \left(C_2 - \frac{C_1^2}{2}\right) \tilde{\alpha}_s^2 + O(\alpha_s^3), \quad (31)$$

and

$$\ln R^{O(\alpha_s^2)}(y, \alpha_s) = \mathcal{A}(y)\tilde{\alpha}_s + \left(\mathcal{B}(y) - \frac{\mathcal{A}(y)^2}{2}\right) \tilde{\alpha}_s^2 + O(\alpha_s^3). \quad (32)$$

Adding Eqs. (31) and (32), and subtracting the overlapping first- and second-order terms from Eq. (31), yields [10,11]

$$\ln R^{\text{resum}+O(\alpha_s^2)}(y, \alpha_s) = \Sigma^{\text{resum}}(\alpha_s, L) - \Sigma^{\text{resum}(1)}(\alpha_s, L) - \Sigma^{\text{resum}(2)}(\alpha_s, L) + \mathcal{A}(y)\tilde{\alpha}_s + \left(\mathcal{B}(y) - \frac{\mathcal{A}^2(y)}{2}\right) \tilde{\alpha}_s^2, \quad (33)$$

where

$$\Sigma^{\text{resum}(1)}(\alpha_s, L) = G_{12}\tilde{\alpha}_s L^2 + G_{11}\tilde{\alpha}_s L, \quad (34)$$

$$\Sigma^{\text{resum}(2)}(\alpha_s, L) = G_{23}\tilde{\alpha}_s^2 L^3 + G_{22}\tilde{\alpha}_s^2 L^2. \quad (35)$$

Finally, one can derive $R^{\text{resum}+O(\alpha_s^2)}(y, \alpha_s)$ by taking the exponential of Eq. (33). This procedure is called *lnR matching*.

In an alternative approach, the overlapping terms $\Sigma^{\text{resum}(1)}(\alpha_s, L)$ and $\Sigma^{\text{resum}(2)}(\alpha_s, L)$ are subtracted from $\Sigma^{\text{resum}}(\alpha_s, L)$ in the form of an exponential. The exact formula up to $O(\alpha_s^2)$ is then obtained as follows [14,15]:

$$\begin{aligned} R^{\text{resum}+O(\alpha_s^2)}(y, \alpha_s) &= (1 + C_1 \tilde{\alpha}_s + C_2 \tilde{\alpha}_s^2) [\exp\{\Sigma^{\text{resum}}(\alpha_s, L)\} - \exp\{\Sigma^{\text{resum}(1)}(\alpha_s, L) + \Sigma^{\text{resum}(2)}(\alpha_s, L)\}] \\ &\quad + 1 + \mathcal{A}(y)\tilde{\alpha}_s + \mathcal{B}(y)\tilde{\alpha}_s^2 \\ &= (1 + C_1 \tilde{\alpha}_s + C_2 \tilde{\alpha}_s^2) \exp\{\Sigma^{\text{resum}}(\alpha_s, L)\} - [C_1 \tilde{\alpha}_s + \Sigma^{\text{resum}(1)}(\alpha_s, L)] \\ &\quad - [C_2 \tilde{\alpha}_s^2 + C_1 \tilde{\alpha}_s \Sigma^{\text{resum}(1)}(\alpha_s, L) + \frac{1}{2} \{\Sigma^{\text{resum}(1)}(\alpha_s, L)\}^2 + \Sigma^{\text{resum}(2)}(\alpha_s, L)] \\ &\quad + \mathcal{A}(y)\tilde{\alpha}_s + \mathcal{B}(y)\tilde{\alpha}_s^2. \end{aligned} \quad (36)$$

This is called *R matching*, and differs from *lnR matching* in that the subleading term $G_{21}\tilde{\alpha}_s^2 L$ is not exponentiated. In order to raise this procedure to the same level as the *lnR matching* scheme, Eq. (36) may be modified by replacing $\Sigma^{\text{resum}}(\alpha_s, L)$ and $\Sigma^{\text{resum}(2)}(\alpha_s, L)$ with $\Sigma(\alpha_s, L)$ and

$$\Sigma^{(2)}(\alpha_s, L) = G_{23}\tilde{\alpha}_s^2 L^3 + G_{22}\tilde{\alpha}_s^2 L^2 + G_{21}\tilde{\alpha}_s^2 L,$$

respectively. This procedure is called *modified R matching*¹ [14].

¹It has also been called *R-G₂₁ matching* [30], or *intermediate matching* [31].

The predictions of these matching schemes have some troublesome features near the upper kinematic limit y_{max} because terms of third and higher order generated by the resummed calculations do not vanish at this limit. This situation can be corrected by invoking a replacement of $L = \ln(1/y)$ in Eq. (33) with $L' = \ln(1/y - 1/y_{\text{max}} + 1)$. This procedure is called *modified lnR matching* [32]. We took the value of y_{max} to be 0.5 for τ , 0.42 for ρ , 0.41 for B_T , 0.325 for B_W , and 0.33 for $D_2(D)$.

Finally, in order to account for the renormalization scale dependence, $f_{\text{NLL}}(\alpha_s L)$ should be modified to

$$f_{\text{NLL}}(\alpha_s L) + (\alpha_s L)^2 \frac{df_{\text{LL}}(\alpha_s L)}{d(\alpha_s L)} b_0 \ln f,$$

and $\mathcal{B}(y)$ and G_{22} should be modified to $\mathcal{B}(y) + \mathcal{A}(y)2\pi b_0 \ln f$ and $G_{22} + G_{12}2\pi b_0 \ln f$, respectively [7,15].

V. MEASUREMENT OF $\alpha_s(M_Z^2)$

A. Data analysis

The 15 observables defined in Sec. III were calculated from the experimental data using charged tracks in hadronic events selected according to the criteria defined in Sec. II. The experimental distributions $D_{\text{SLD}}^{\text{data}}(y)$ were then corrected for the effects of selection cuts, detector acceptance, efficiency, and resolution, for neutral particles, particle decays, and interactions within the detector, and for initial-state photon radiation, using bin-by-bin correction factors $C_D(y)$:

$$C_D(y)_i = \frac{D_{\text{hadron}}^{\text{MC}}(y)_i}{D_{\text{SLD}}^{\text{MC}}(y)_i}, \quad (37)$$

where y is the observable; i is the bin index; $D_{\text{SLD}}^{\text{MC}}(y)_i$ is the content of bin i of the distribution obtained from reconstructed charged particles in Monte Carlo events after simulation of the detector; and $D_{\text{hadron}}^{\text{MC}}(y)_i$ is that from all generated particles with lifetimes greater than 3×10^{-10} s in Monte Carlo events with no SLD simulation and no initial-state radiation. The bin widths were chosen from the estimated experimental resolution so as to minimize bin-to-bin migration effects. The $C_D(y)$ were calculated using events generated with JETSET 6.3 [21] using parameter values tuned to hadronic e^+e^- annihilation data [33]. In addition, the multiplicity and momentum spectra of B hadron decay products were tuned to Υ_{4S} data [34]. The *hadron level* distributions are then given by

$$D_{\text{hadron}}^{\text{data}}(y)_i = C_D(y)_i D_{\text{SLD}}^{\text{data}}(y)_i. \quad (38)$$

Systematic effects were investigated using a variety of techniques. The experimental systematic errors arising from uncertainties in modeling the detector were estimated by varying the charged track and event selection criteria over wide ranges, and by varying the tracking efficiency and resolution in the detector simulation. In each case the correction factors $C_D(y)$, and hence the corrected data distributions $D_{\text{hadron}}^{\text{data}}(y)$, were rederived. The data correction procedure was repeated by recalculating the correction factors $C_D(y)$ using events generated with HERWIG 5.5 [22]. In addition, a matrix correction procedure [35] was employed, in which migrations between all pairs of bins are accounted for individually. The differences between the data distributions corrected by the bin-by-bin and matrix methods were found to be much smaller than the statistical errors.

The hadron level data are shown in Figs. 1–15 and listed in Tables I–VII, together with statistical and systematic errors; they may be compared with data from other experiments that have applied corrections for detector effects. The central values represent the data corrected by the central values of the correc-

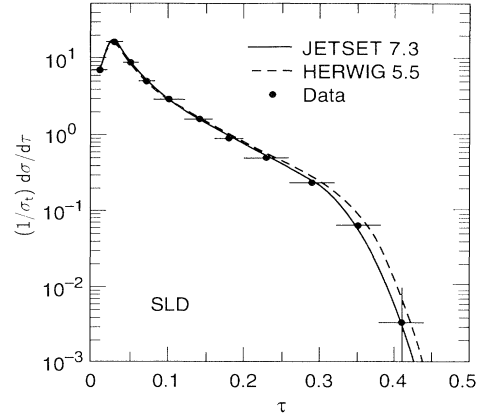


FIG. 1. The measured thrust distribution corrected to the hadron level. The error bars include the statistical and experimental systematic errors added in quadrature. The curves show the predictions of the QCD parton shower models JETSET 7.3 (solid line) and HERWIG 5.5 (dashed line).

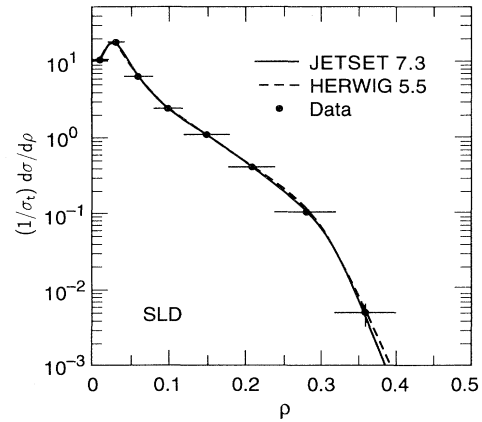


FIG. 2. The same as Fig. 1 but for the heavy jet mass.

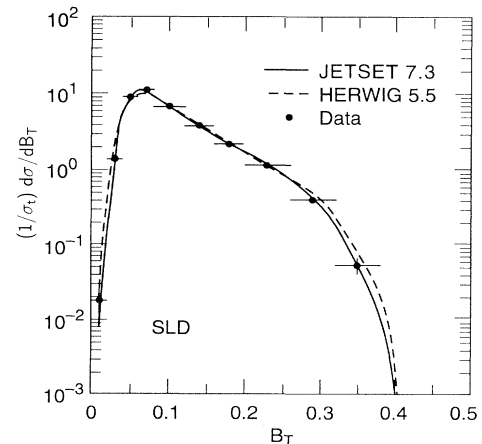


FIG. 3. The same as Fig. 1 but for the total jet broadening.

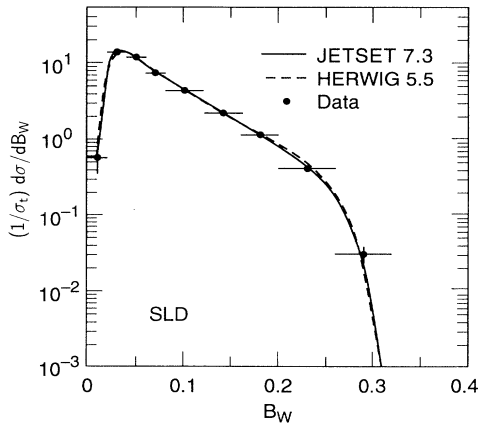


FIG. 4. The same as Fig. 1 but for the wide jet broadening.

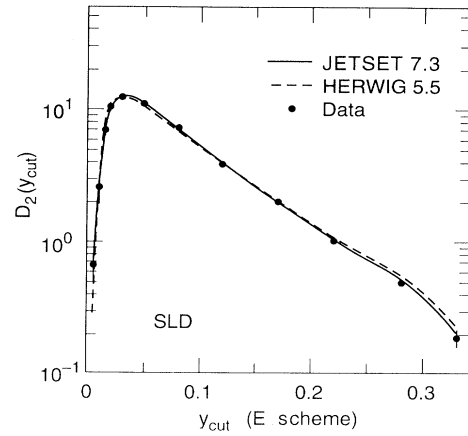
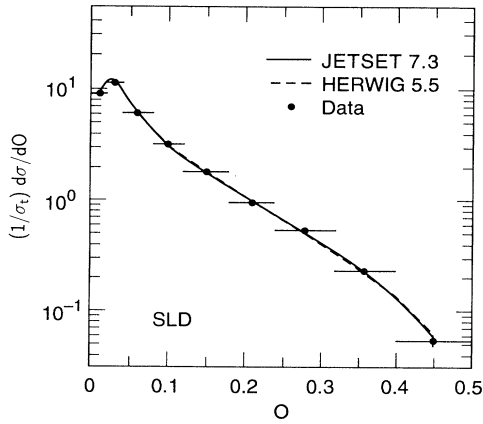
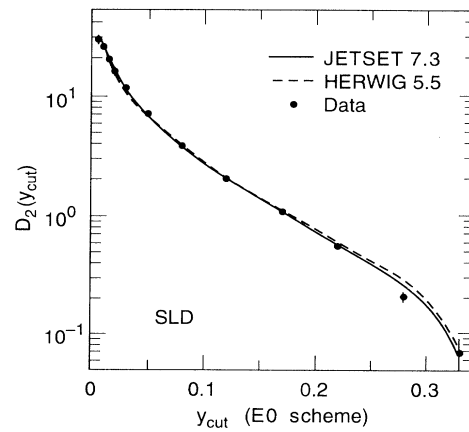
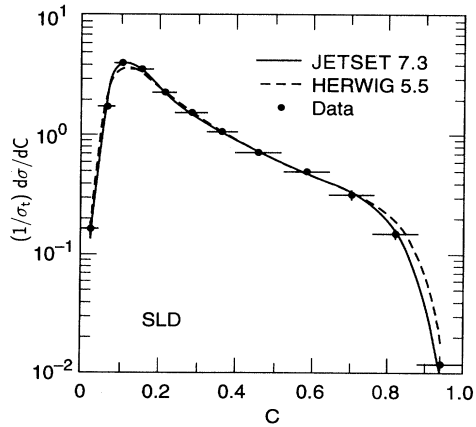
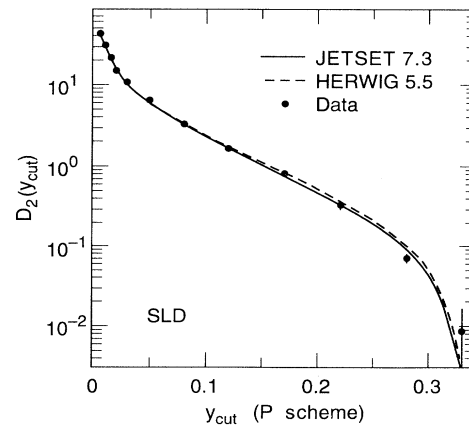
FIG. 7. The same as Fig. 1 but for the differential two-jet rate with the E scheme.

FIG. 5. The same as Fig. 1 but for the oblateness.

FIG. 8. The same as Fig. 1 but for the differential two-jet rate with the $E0$ scheme.FIG. 6. The same as Fig. 1 but for the C parameter.FIG. 9. The same as Fig. 1 but for the differential two-jet rate with the P scheme.

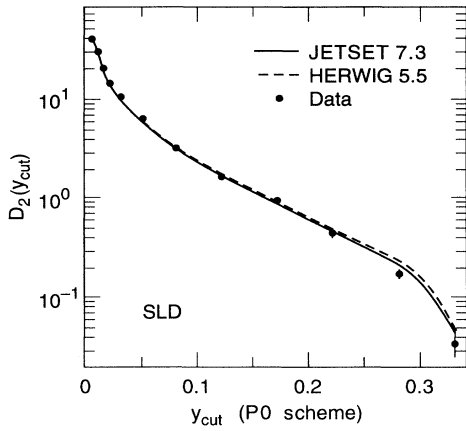


FIG. 10. The same as Fig. 1 but for the differential two-jet rate with the P_0 scheme.

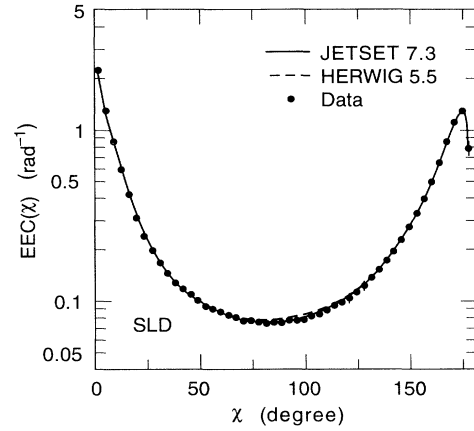


FIG. 13. The same as Fig. 1 but for the energy-energy correlation (EEC).

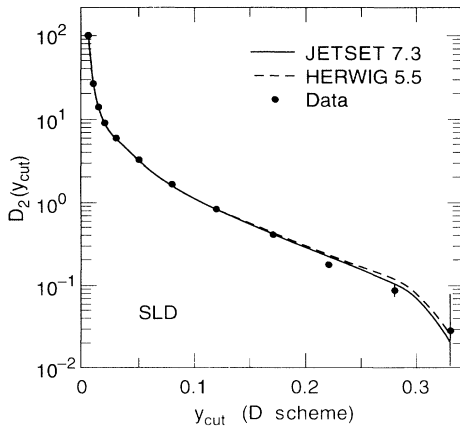


FIG. 11. The same as Fig. 1 but for the differential two-jet rate with the D scheme.

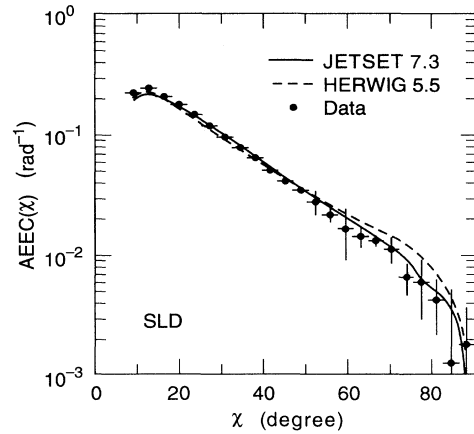


FIG. 14. The same as Fig. 1 but for the asymmetry of the energy-energy correlation (AECC).

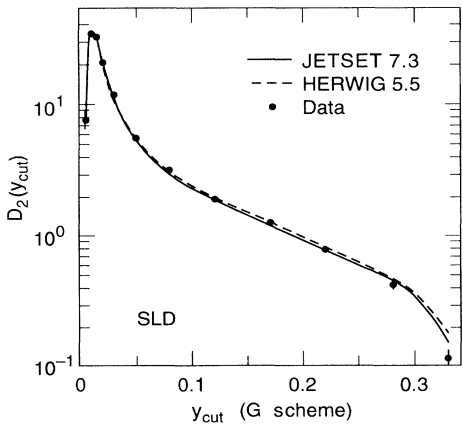


FIG. 12. The same as Fig. 1 but for the differential two-jet rate with the G scheme.

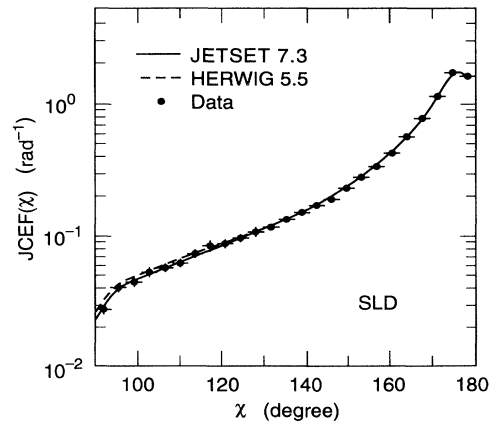


FIG. 15. The same as Fig. 1 but for the jet cone energy fraction (JCEF).

TABLE I. Distributions of τ and ρ (see text). The data were corrected for detector effects and for initial state photon radiation. The first error is statistical, and the second represents the experimental systematic uncertainty.

τ	$\frac{1}{\sigma_t} \frac{d\sigma}{d\tau} \pm (\text{stat}) \pm (\text{expt syst})$	ρ	$\frac{1}{\sigma_t} \frac{d\sigma}{d\rho} \pm (\text{stat}) \pm (\text{expt syst})$
0.0 – 0.02	$7.01 \pm 0.10 \pm 0.50$	0.0 – 0.02	$10.53 \pm 0.12 \pm 0.41$
0.02 – 0.04	$16.10 \pm 0.15 \pm 0.15$	0.02 – 0.04	$17.38 \pm 0.15 \pm 0.14$
0.04 – 0.06	$8.67 \pm 0.11 \pm 0.05$	0.04 – 0.08	$6.21 \pm 0.07 \pm 0.16$
0.06 – 0.08	$5.08 \pm 0.08 \pm 0.16$	0.08 – 0.12	$2.39 \pm 0.04 \pm 0.09$
0.08 – 0.12	$2.91 \pm 0.04 \pm 0.06$	0.12 – 0.18	$1.08 \pm 0.02 \pm 0.04$
0.12 – 0.16	$1.57 \pm 0.03 \pm 0.05$	0.18 – 0.24	$0.404 \pm 0.014 \pm 0.021$
0.16 – 0.20	$0.917 \pm 0.025 \pm 0.028$	0.24 – 0.32	$0.102 \pm 0.006 \pm 0.010$
0.20 – 0.26	$0.495 \pm 0.015 \pm 0.025$	0.32 – 0.40	$0.0047 \pm 0.0013 \pm 0.0008$
0.26 – 0.32	$0.227 \pm 0.010 \pm 0.016$		
0.32 – 0.38	$0.061 \pm 0.005 \pm 0.006$		
0.38 – 0.44	$0.003 \pm 0.001 \pm 0.003$		

TABLE II. Distributions of B_T and B_W (see text). The data were corrected for detector effects and for initial-state photon radiation. The first error is statistical, and the second represents the experimental systematic uncertainty.

B_T	$\frac{1}{\sigma_t} \frac{d\sigma}{dB_T} \pm (\text{stat}) \pm (\text{expt syst})$	B_W	$\frac{1}{\sigma_t} \frac{d\sigma}{dB_W} \pm (\text{stat}) \pm (\text{expt syst})$
0.0 – 0.02	$0.018 \pm 0.005 \pm 0.007$	0.0 – 0.02	$0.570 \pm 0.028 \pm 0.213$
0.02 – 0.04	$1.36 \pm 0.04 \pm 0.18$	0.02 – 0.04	$13.86 \pm 0.14 \pm 0.45$
0.04 – 0.06	$8.81 \pm 0.11 \pm 0.32$	0.04 – 0.06	$11.71 \pm 0.13 \pm 0.20$
0.06 – 0.08	$10.64 \pm 0.12 \pm 0.16$	0.06 – 0.08	$7.38 \pm 0.10 \pm 0.11$
0.08 – 0.12	$6.52 \pm 0.07 \pm 0.10$	0.08 – 0.12	$4.29 \pm 0.05 \pm 0.08$
0.12 – 0.16	$3.65 \pm 0.05 \pm 0.04$	0.12 – 0.16	$2.185 \pm 0.038 \pm 0.128$
0.16 – 0.20	$2.10 \pm 0.04 \pm 0.06$	0.16 – 0.20	$1.12 \pm 0.028 \pm 0.061$
0.20 – 0.26	$1.12 \pm 0.02 \pm 0.03$	0.20 – 0.26	$0.403 \pm 0.014 \pm 0.025$
0.26 – 0.32	$0.384 \pm 0.013 \pm 0.023$	0.26 – 0.32	$0.030 \pm 0.004 \pm 0.005$
0.32 – 0.38	$0.050 \pm 0.005 \pm 0.011$		

TABLE III. Distributions of O and C (see text). The data were corrected for detector effects and for initial-state photon radiation. The first error is statistical, and the second represents the experimental systematic uncertainty.

O	$\frac{1}{\sigma_t} \frac{d\sigma}{dO} \pm (\text{stat}) \pm (\text{expt syst})$	C	$\frac{1}{\sigma_t} \frac{d\sigma}{dC} \pm (\text{stat}) \pm (\text{expt syst})$
0.0 – 0.02	$9.07 \pm 0.11 \pm 0.19$	0.0 – 0.04	$0.166 \pm 0.011 \pm 0.015$
0.20 – 0.04	$11.28 \pm 0.12 \pm 0.20$	0.04 – 0.08	$1.76 \pm 0.03 \pm 0.04$
0.04 – 0.08	$5.98 \pm 0.06 \pm 0.07$	0.08 – 0.12	$4.01 \pm 0.05 \pm 0.09$
0.08 – 0.12	$3.16 \pm 0.05 \pm 0.06$	0.12 – 0.18	$3.57 \pm 0.04 \pm 0.10$
0.12 – 0.18	$1.77 \pm 0.03 \pm 0.03$	0.18 – 0.24	$2.30 \pm 0.03 \pm 0.02$
0.18 – 0.24	$0.935 \pm 0.021 \pm 0.028$	0.24 – 0.32	$1.54 \pm 0.02 \pm 0.016$
0.24 – 0.32	$0.523 \pm 0.013 \pm 0.013$	0.32 – 0.40	$1.07 \pm 0.02 \pm 0.03$
0.32 – 0.40	$0.223 \pm 0.009 \pm 0.010$	0.40 – 0.52	$0.718 \pm 0.013 \pm 0.024$
0.40 – 0.50	$0.052 \pm 0.004 \pm 0.003$	0.52 – 0.64	$0.491 \pm 0.011 \pm 0.013$
		0.64 – 0.76	$0.311 \pm 0.008 \pm 0.022$
		0.76 – 0.88	$0.146 \pm 0.006 \pm 0.012$
		0.88 – 1.0	$0.012 \pm 0.002 \pm 0.001$

TABLE IV. $D_2(y_{\text{cut}})$ calculated in the E scheme, the $E0$ scheme, and the P scheme (see text). The data were corrected for detector effects and for initial-state photon radiation. The first error is statistical, and the second represents the experimental systematic uncertainty.

y_{cut}	E scheme $D_2(y_{\text{cut}}) \pm (\text{stat}) \pm (\text{expt syst})$	$E0$ scheme $D_2(y_{\text{cut}}) \pm (\text{stat}) \pm (\text{expt syst})$	P scheme $D_2(y_{\text{cut}}) \pm (\text{stat}) \pm (\text{expt syst})$
0.005	$0.669 \pm 0.060 \pm 0.080$	$28.95 \pm 0.39 \pm 1.44$	$41.80 \pm 0.47 \pm 2.43$
0.010	$2.60 \pm 0.12 \pm 0.12$	$25.25 \pm 0.37 \pm 0.50$	$31.06 \pm 0.41 \pm 0.63$
0.015	$7.07 \pm 0.20 \pm 0.27$	$19.93 \pm 0.33 \pm 0.53$	$21.24 \pm 0.34 \pm 0.28$
0.02	$10.48 \pm 0.24 \pm 0.66$	$15.85 \pm 0.29 \pm 1.04$	$14.96 \pm 0.28 \pm 0.54$
0.03	$12.28 \pm 0.18 \pm 0.39$	$11.66 \pm 0.18 \pm 0.15$	$10.82 \pm 0.17 \pm 0.37$
0.05	$10.89 \pm 0.12 \pm 0.34$	$7.01 \pm 0.10 \pm 0.19$	$6.35 \pm 0.09 \pm 0.23$
0.08	$7.22 \pm 0.08 \pm 0.22$	$3.85 \pm 0.06 \pm 0.05$	$3.16 \pm 0.05 \pm 0.09$
0.12	$3.81 \pm 0.05 \pm 0.11$	$2.02 \pm 0.04 \pm 0.07$	$1.61 \pm 0.03 \pm 0.08$
0.17	$1.97 \pm 0.03 \pm 0.05$	$1.08 \pm 0.02 \pm 0.04$	$0.791 \pm 0.021 \pm 0.037$
0.22	$0.987 \pm 0.023 \pm 0.034$	$0.537 \pm 0.017 \pm 0.026$	$0.317 \pm 0.013 \pm 0.024$
0.28	$0.467 \pm 0.015 \pm 0.017$	$0.204 \pm 0.010 \pm 0.015$	$0.069 \pm 0.006 \pm 0.005$
0.33	$0.178 \pm 0.009 \pm 0.024$	$0.068 \pm 0.006 \pm 0.021$	$0.008 \pm 0.002 \pm 0.007$

tion factors $C_D(y)$, which are shown in Figs. 16(c)–30(c). For the EEC, AEEC, and JCEF, where there are bin-to-bin correlations and multiple entries per event per bin, the statistical error in each bin was estimated by taking the rms deviation of the contents of that bin over 50 Monte Carlo samples, each comprising the same number of events as the data sample. The systematic errors derive from the uncertainties on the correction factors shown in Figs. 16(c)–30(c). Also shown in Figs. 1–15 are the predictions of the JETSET 7.3 [36] and HERWIG 5.5 [22] QCD + fragmentation event generators. Good agreement between the data and model predictions is apparent in all cases.

Before they can be compared with the QCD predictions, the data must be corrected for the effects of hadronization. The correction procedure is similar to that described above for the detector effects. Bin-by-bin correction factors

$$C_H(y)_i = \frac{D_{\text{parton}}^{\text{MC}}(y)_i}{D_{\text{hadron}}^{\text{MC}}(y)_i}, \quad (39)$$

where $D_{\text{parton}}^{\text{MC}}(y)_i$ is the content of bin i of the distribution obtained from Monte Carlo events generated at the parton level, were calculated and applied to the hadron level data distributions $D_{\text{hadron}}^{\text{data}}(y)_i$ to obtain the *parton level* corrected data:

$$D_{\text{parton}}^{\text{data}}(y)_i = C_H(y)_i D_{\text{hadron}}^{\text{data}}(y)_i. \quad (40)$$

The phenomenological hadronization models implemented in JETSET 7.3 and HERWIG 5.5 were used to calculate the $C_H(y)$. In the case of JETSET the $C_H(y)$ were also recalculated for values of the parton virtuality cutoff Q_0 [21,36] in the range 0.5–2.0 GeV, and for reasonable variations of the parameters Λ_{LL} , a , and σ_q . The correction factors $C_H(y)$ are shown in Figs. 16(b)–30(b), where the bands show the uncertainties due to model differences and parameter variations. The parton level data are shown in Figs. 16(a)–30(a). The data points correspond to the central values of the hadronization correction factors, and the errors shown are statistical and experimental systematic only; the hadronization uncer-

TABLE V. $D_2(y_{\text{cut}})$ calculated in the $P0$ scheme, the D scheme, and the G scheme (see text). The data were corrected for detector effects and for initial-state photon radiation. The first error is statistical, and the second represents the experimental systematic uncertainty.

y_{cut}	$P0$ scheme $D_2(y_{\text{cut}}) \pm (\text{stat}) \pm (\text{expt syst})$	D scheme $D_2(y_{\text{cut}}) \pm (\text{stat}) \pm (\text{expt syst})$	G scheme $D_2(y_{\text{cut}}) \pm (\text{stat}) \pm (\text{expt syst})$
0.005	$39.78 \pm 0.46 \pm 2.41$	$101.06 \pm 0.74 \pm 2.29$	$7.67 \pm 0.20 \pm 1.01$
0.010	$29.85 \pm 0.40 \pm 0.78$	$26.85 \pm 0.38 \pm 0.34$	$33.63 \pm 0.43 \pm 0.84$
0.015	$20.49 \pm 0.33 \pm 0.36$	$14.13 \pm 0.28 \pm 0.40$	$31.71 \pm 0.41 \pm 1.01$
0.02	$14.52 \pm 0.28 \pm 0.23$	$9.00 \pm 0.22 \pm 0.44$	$20.46 \pm 0.33 \pm 0.55$
0.03	$10.65 \pm 0.17 \pm 0.37$	$6.02 \pm 0.13 \pm 0.17$	$11.71 \pm 0.18 \pm 0.20$
0.05	$6.36 \pm 0.09 \pm 0.19$	$3.30 \pm 0.07 \pm 0.11$	$5.55 \pm 0.09 \pm 0.12$
0.08	$3.21 \pm 0.05 \pm 0.12$	$1.66 \pm 0.04 \pm 0.07$	$3.20 \pm 0.05 \pm 0.06$
0.12	$1.64 \pm 0.03 \pm 0.07$	$0.831 \pm 0.024 \pm 0.038$	$1.92 \pm 0.04 \pm 0.05$
0.17	$0.944 \pm 0.023 \pm 0.057$	$0.406 \pm 0.015 \pm 0.033$	$1.25 \pm 0.03 \pm 0.03$
0.22	$0.433 \pm 0.015 \pm 0.038$	$0.173 \pm 0.010 \pm 0.011$	$0.768 \pm 0.020 \pm 0.027$
0.28	$0.169 \pm 0.009 \pm 0.015$	$0.084 \pm 0.006 \pm 0.013$	$0.409 \pm 0.014 \pm 0.019$
0.33	$0.034 \pm 0.004 \pm 0.008$	$0.027 \pm 0.004 \pm 0.048$	$0.111 \pm 0.007 \pm 0.018$

TABLE VI. The EEC (see text). The data were corrected for detector effects and for initial-state photon radiation. The first error is statistical, and the second represents the experimental systematic uncertainty.

χ (deg)	EEC (rad^{-1}) \pm (stat) \pm (expt syst)	χ (deg)	EEC (rad^{-1}) \pm (stat) \pm (expt syst)
0.0 – 3.6	2.265 \pm 0.006 \pm 0.055	90.0 – 93.6	0.0761 \pm 0.0009 \pm 0.0013
3.6 – 7.2	1.316 \pm 0.006 \pm 0.032	93.6 – 97.2	0.0764 \pm 0.0009 \pm 0.0025
7.2 – 10.8	0.874 \pm 0.004 \pm 0.020	97.2 – 100.8	0.0777 \pm 0.0009 \pm 0.0023
10.8 – 14.4	0.598 \pm 0.003 \pm 0.019	100.8 – 104.4	0.0809 \pm 0.0012 \pm 0.0016
14.4 – 18.0	0.425 \pm 0.002 \pm 0.011	104.4 – 108.0	0.0834 \pm 0.0010 \pm 0.0024
18.0 – 21.6	0.310 \pm 0.002 \pm 0.014	108.0 – 111.6	0.0874 \pm 0.0010 \pm 0.0022
21.6 – 25.2	0.241 \pm 0.001 \pm 0.005	111.6 – 115.2	0.0931 \pm 0.0013 \pm 0.0015
25.2 – 28.8	0.199 \pm 0.001 \pm 0.005	115.2 – 118.8	0.0968 \pm 0.0012 \pm 0.0038
28.8 – 32.4	0.168 \pm 0.001 \pm 0.006	118.8 – 122.4	0.1030 \pm 0.0012 \pm 0.0070
32.4 – 36.0	0.146 \pm 0.001 \pm 0.005	122.4 – 126.0	0.111 \pm 0.001 \pm 0.002
36.0 – 39.6	0.128 \pm 0.001 \pm 0.004	126.0 – 129.6	0.121 \pm 0.001 \pm 0.007
39.6 – 43.2	0.118 \pm 0.001 \pm 0.003	129.6 – 133.2	0.136 \pm 0.002 \pm 0.003
43.2 – 46.8	0.1099 \pm 0.0008 \pm 0.0026	133.2 – 136.8	0.151 \pm 0.002 \pm 0.004
46.8 – 50.4	0.1014 \pm 0.0009 \pm 0.0031	136.8 – 140.4	0.170 \pm 0.002 \pm 0.005
50.4 – 54.0	0.0935 \pm 0.0008 \pm 0.0027	140.4 – 144.0	0.193 \pm 0.002 \pm 0.006
54.0 – 57.6	0.0901 \pm 0.0009 \pm 0.0021	144.0 – 147.2	0.225 \pm 0.002 \pm 0.008
57.6 – 61.2	0.0867 \pm 0.0008 \pm 0.0023	147.2 – 151.2	0.265 \pm 0.002 \pm 0.007
61.2 – 64.8	0.0827 \pm 0.0009 \pm 0.0023	151.2 – 154.8	0.320 \pm 0.003 \pm 0.008
64.8 – 68.4	0.0802 \pm 0.0010 \pm 0.0018	154.8 – 158.4	0.390 \pm 0.003 \pm 0.013
68.4 – 72.0	0.0764 \pm 0.0009 \pm 0.0031	158.4 – 162.0	0.491 \pm 0.003 \pm 0.017
72.0 – 75.6	0.0770 \pm 0.0010 \pm 0.0010	162.0 – 165.6	0.636 \pm 0.004 \pm 0.012
75.6 – 79.2	0.0752 \pm 0.0008 \pm 0.0031	165.6 – 169.2	0.847 \pm 0.006 \pm 0.007
79.2 – 82.8	0.0736 \pm 0.0008 \pm 0.0013	169.2 – 172.8	1.098 \pm 0.005 \pm 0.009
82.8 – 86.4	0.0751 \pm 0.0010 \pm 0.0015	172.8 – 176.4	1.276 \pm 0.007 \pm 0.044
86.4 – 90.0	0.0744 \pm 0.0010 \pm 0.0014	176.4 – 180.0	0.764 \pm 0.007 \pm 0.050

TABLE VII. The AEEC and JCEF (see text). The data were corrected for detector effects and for initial-state photon radiation. The first error is statistical, and the second represents the experimental systematic uncertainty.

χ (deg)	AEEC (rad^{-1}) \pm (stat) \pm (expt syst)	χ (deg)	JCEF (rad^{-1}) \pm (stat) \pm (expt syst)
0.0 – 3.6		90.0 – 93.6	0.0274 \pm 0.0016 \pm 0.0010
3.6 – 7.2		93.6 – 97.2	0.0403 \pm 0.0020 \pm 0.0012
7.2 – 10.8	0.224 \pm 0.010 \pm 0.002	97.2 – 100.8	0.0442 \pm 0.0026 \pm 0.0010
10.8 – 14.4	0.249 \pm 0.009 \pm 0.005	100.8 – 104.4	0.0523 \pm 0.0029 \pm 0.0023
14.4 – 18.0	0.211 \pm 0.006 \pm 0.005	104.4 – 108.0	0.0566 \pm 0.0029 \pm 0.0024
18.0 – 21.6	0.181 \pm 0.004 \pm 0.005	108.0 – 111.6	0.0613 \pm 0.0034 \pm 0.0026
21.6 – 25.2	0.148 \pm 0.004 \pm 0.006	111.6 – 115.2	0.0725 \pm 0.0039 \pm 0.0017
25.2 – 28.8	0.121 \pm 0.003 \pm 0.004	115.2 – 118.8	0.0832 \pm 0.0055 \pm 0.0046
28.8 – 32.4	0.0972 \pm 0.0024 \pm 0.0029	118.8 – 122.4	0.0858 \pm 0.0051 \pm 0.0016
32.4 – 36.0	0.0785 \pm 0.0022 \pm 0.0062	122.4 – 126.0	0.0944 \pm 0.0043 \pm 0.0024
36.0 – 39.6	0.0645 \pm 0.0017 \pm 0.0024	126.0 – 129.6	0.1051 \pm 0.0061 \pm 0.0055
39.6 – 43.2	0.0513 \pm 0.0020 \pm 0.0026	129.6 – 133.2	0.114 \pm 0.005 \pm 0.002
43.2 – 46.8	0.0413 \pm 0.0015 \pm 0.0027	133.2 – 136.8	0.131 \pm 0.005 \pm 0.005
46.8 – 50.4	0.0346 \pm 0.0016 \pm 0.0021	136.8 – 140.4	0.148 \pm 0.005 \pm 0.006
50.4 – 54.0	0.0275 \pm 0.0013 \pm 0.0060	140.4 – 144.0	0.169 \pm 0.007 \pm 0.004
54.0 – 57.6	0.0213 \pm 0.0010 \pm 0.0024	144.0 – 147.2	0.188 \pm 0.007 \pm 0.005
57.6 – 61.2	0.0163 \pm 0.0008 \pm 0.0073	147.2 – 151.2	0.228 \pm 0.008 \pm 0.009
61.2 – 64.8	0.0141 \pm 0.0007 \pm 0.0026	151.2 – 154.8	0.275 \pm 0.009 \pm 0.010
64.8 – 68.4	0.0129 \pm 0.0010 \pm 0.0008	154.8 – 158.4	0.329 \pm 0.011 \pm 0.013
68.4 – 72.0	0.0110 \pm 0.0007 \pm 0.0025	158.4 – 162.0	0.414 \pm 0.011 \pm 0.019
72.0 – 75.6	0.0064 \pm 0.0005 \pm 0.0017	162.0 – 165.6	0.551 \pm 0.012 \pm 0.013
75.6 – 79.2	0.0058 \pm 0.0006 \pm 0.0029	165.6 – 169.2	0.751 \pm 0.021 \pm 0.021
79.2 – 82.8	0.0041 \pm 0.0004 \pm 0.0020	169.2 – 172.8	1.095 \pm 0.024 \pm 0.019
82.8 – 86.4	0.0012 \pm 0.0002 \pm 0.0038	172.8 – 176.4	1.639 \pm 0.032 \pm 0.034
86.4 – 90.0	0.0017 \pm 0.0008 \pm 0.0016	176.4 – 180.0	1.530 \pm 0.039 \pm 0.049

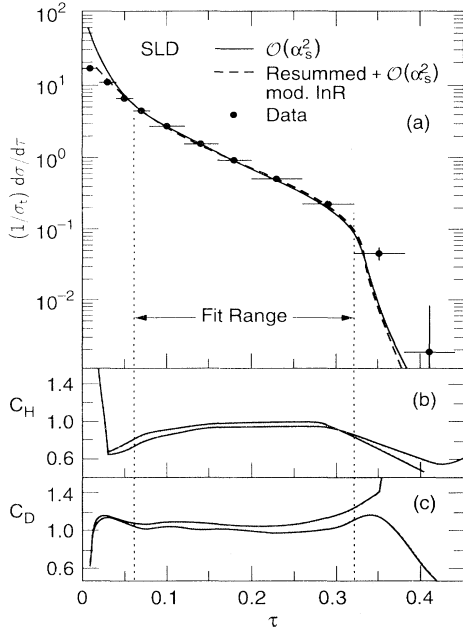


FIG. 16. (a) The measured thrust distribution corrected to the parton level. The error bars include the statistical and experimental systematic errors added in quadrature. The curves show the predictions of the $O(\alpha_s^2)$ calculations (solid line) and the resummed+ $O(\alpha_s^2)$ calculations with modified $\ln R$ matching (dashed line). The renormalization scale factor was fixed to 1. Sizes of the (b) hadronization correction and (c) detector correction factors; the widths of the bands indicate the systematic uncertainties.

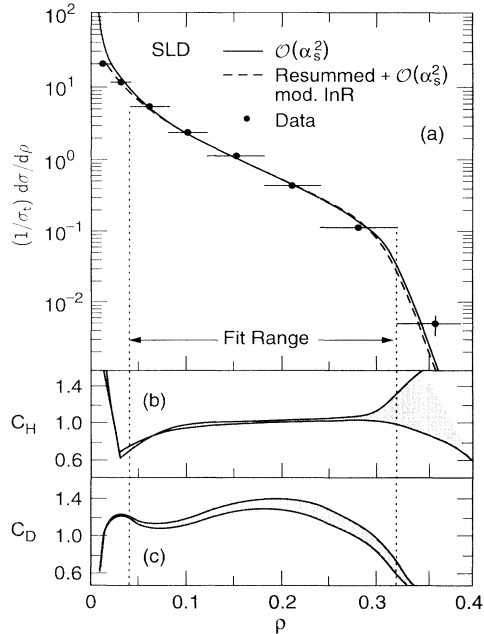


FIG. 17. The same as Fig. 16 but for the heavy jet mass.

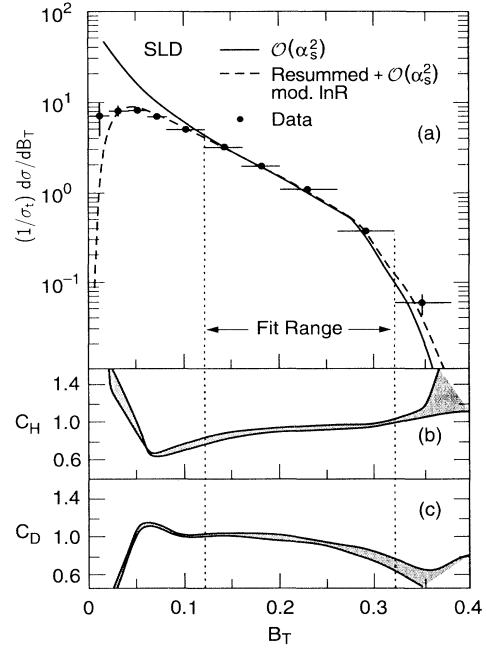


FIG. 18. The same as Fig. 16 but for the total jet broadening.

tainty will be considered in the next sections which describe the fits to determine $\alpha_s(M_Z^2)$.

B. Measurement of $\alpha_s(M_Z^2)$ using $O(\alpha_s^2)$ calculations

We first determined $\alpha_s(M_Z^2)$ by comparing the $O(\alpha_s^2)$ QCD calculations for each observable y with the cor-

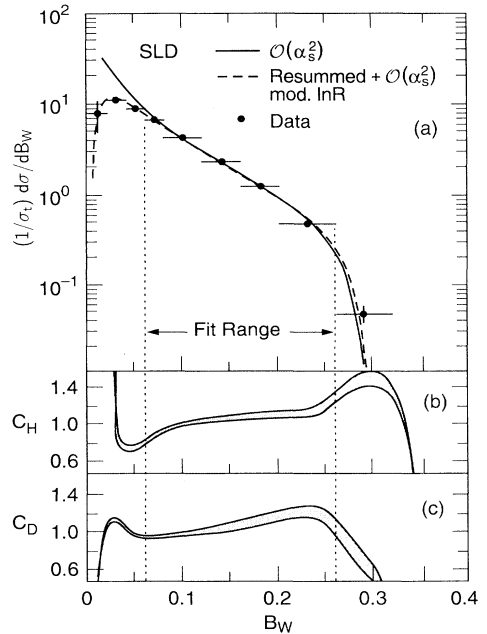


FIG. 19. The same as Fig. 16 but for the wide jet broadening.

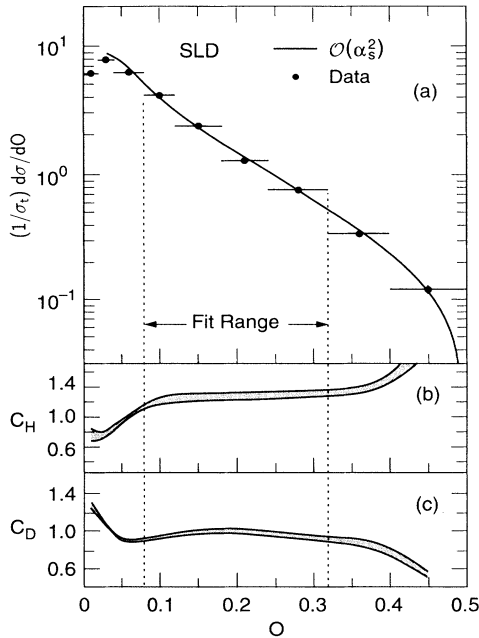
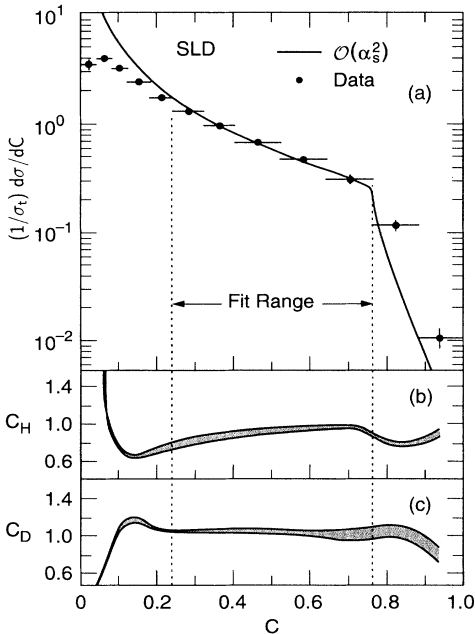
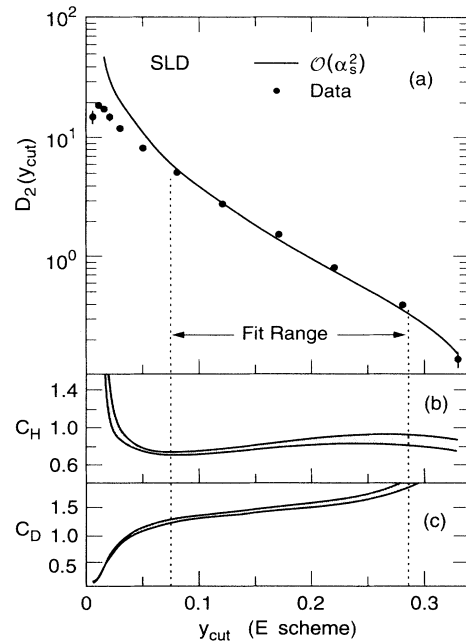
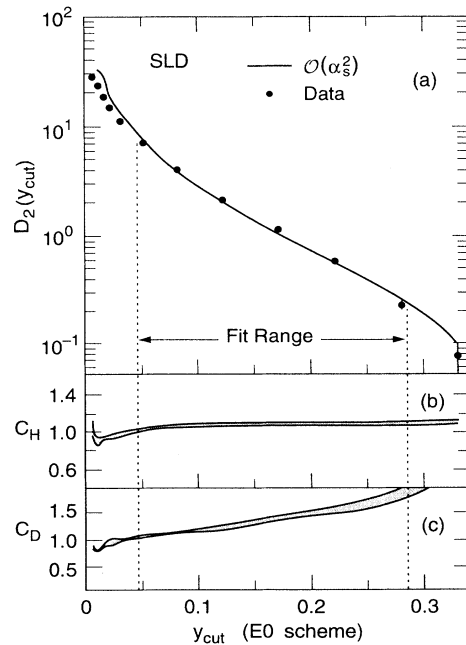


FIG. 20. The same as Fig. 16 but for the oblateness.

rected data at the parton level. Each calculation was fitted to the measured distribution $(1/\sigma_t)(d\sigma/dy)$ by minimizing χ^2 with respect to variation of $\Lambda_{\overline{MS}}$. In each y bin χ^2 was defined using the sum in quadrature of the statistical and systematic errors. Fits were performed at selected values of the scale f and were restricted to the range in y for which the $O(\alpha_s^2)$ calculation provides a good description of the corrected data.

FIG. 21. The same as Fig. 16 but for the C parameter.FIG. 22. The same as Fig. 16 but for the differential two-jet rate with the E scheme.

The fit ranges in y were chosen to ensure that the parton level data and the QCD calculations could be compared meaningfully. The range for each observable was determined according to the following requirements: (1) the hadronization correction factors $C_H(y)$ satisfied $0.6 < C_H(y) < 1.4$; (2) the systematic uncertainties on the detector and hadronization correction factors, $\Delta C_D(y)$ and $\Delta C_H(y)$, respectively, satisfied

FIG. 23. The same as Fig. 16 but for the differential two-jet rate with the $E0$ scheme.

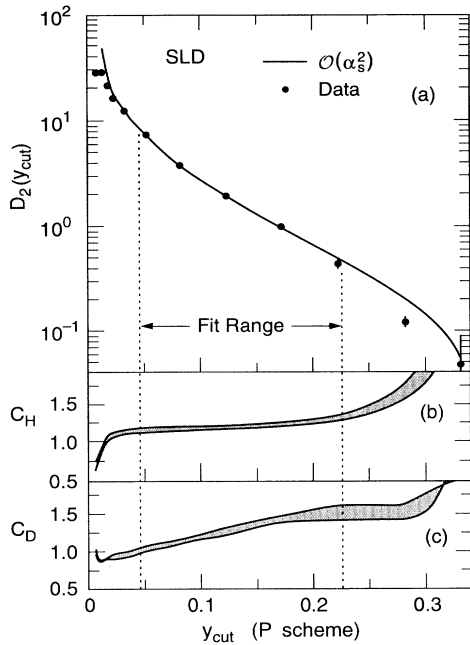


FIG. 24. The same as Fig. 16 but for the differential two-jet rate with the *P* scheme.

$|\Delta C_D(y), \Delta C_H(y)| < 0.3$; (3) three massless partons can contribute to the distribution at $O(\alpha_s)$ in perturbative QCD; (4) the χ^2 per degree of freedom, χ_{DF}^2 , for a fit at $f = 1$ is 5.0 or less. Requirements (1) and (2) ensure that the corrected data are well measured and that the hadronization corrections are modeled reliably. Require-

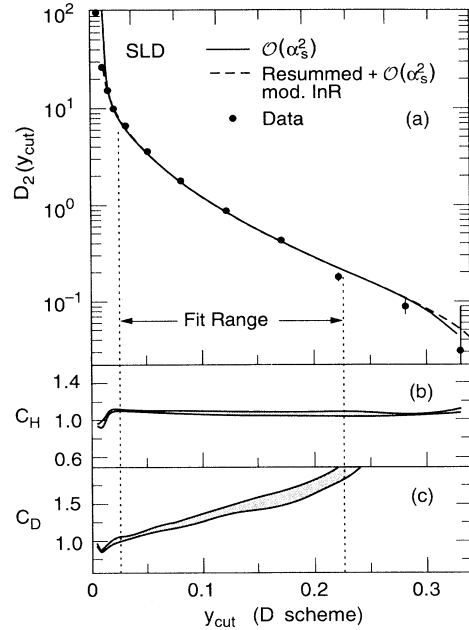


FIG. 26. The same as Fig. 16 but for the differential two-jet rate with the *D* scheme.

ment (3) ensures that the kinematic regions dominated by four-parton production at $O(\alpha_s^2)$ are excluded, as the calculation is effectively leading order, and hence unreliable, in these regions. Requirement (4) is an empirical constraint that ensures that the QCD calculation fits the data reasonably well; this is most relevant to exclude the

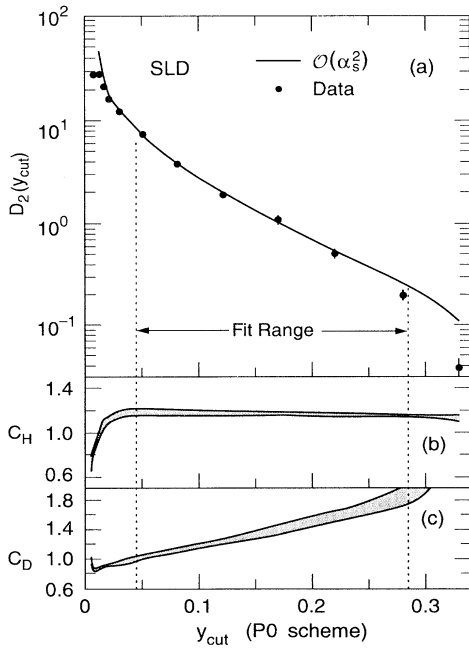


FIG. 25. The same as Fig. 16 but for the differential two-jet rate with the *P0* scheme.

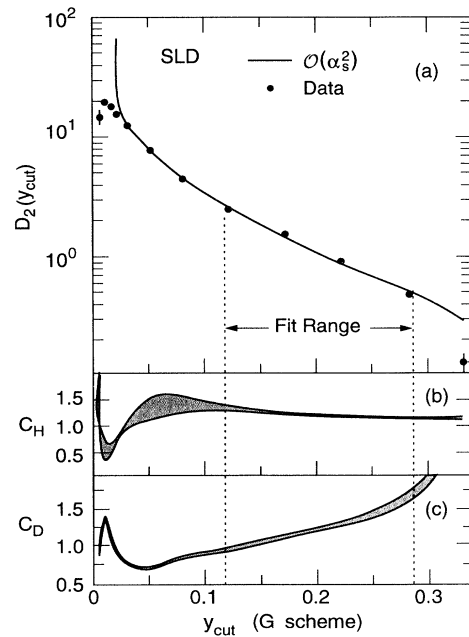


FIG. 27. The same as Fig. 16 but for the differential two-jet rate with the *G* scheme.

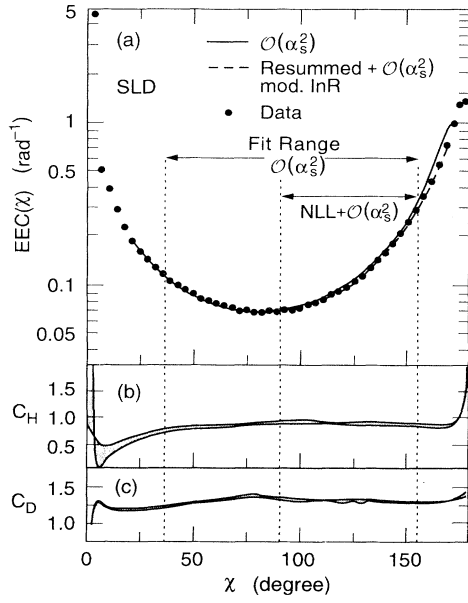


FIG. 28. The same as Fig. 16 but for the energy-energy correlation (EEC).

so-called “two-jet region” where multiple emissions of soft or collinear gluons are important and are not included in the $O(\alpha_s^2)$ calculations, a matter discussed further in Sec. VC. Since the four-jet rate R_4 has been calculated only at leading order, for D_2 the lower bound on y_{cut} was chosen to ensure that R_4 was smaller than 1%. These fit ranges are listed in Table VIII and are shown in Figs. 16–30. For illustration, fits to the distributions are shown in

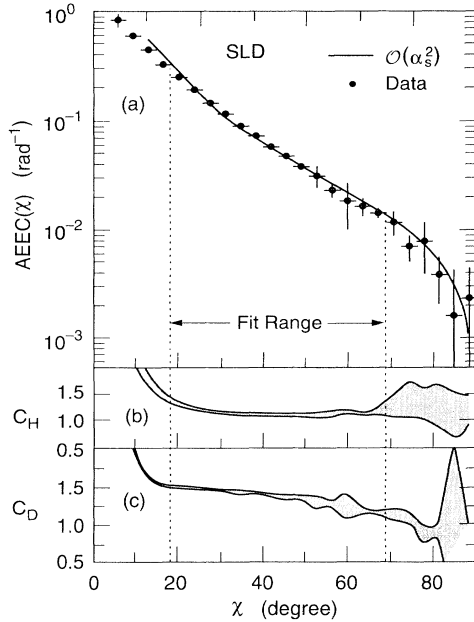


FIG. 29. The same as Fig. 16 but for the asymmetry of the energy-energy correlation (AEEC).

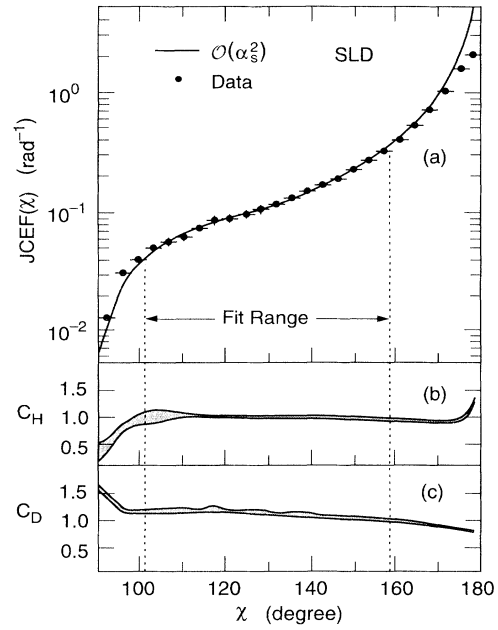


FIG. 30. The same as Fig. 16 but for the jet cone energy fraction (JCEF).

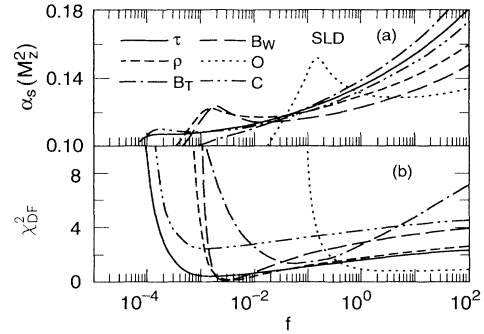


FIG. 31. (a) $\alpha_s(M_Z^2)$ and (b) χ^2_{DF} from the $O(\alpha_s^2)$ fits to the event shapes as a function of renormalization scale factor f (see text).

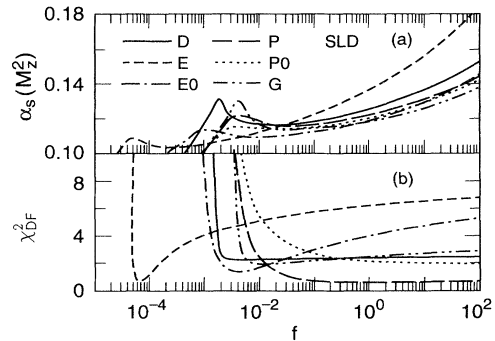


FIG. 32. (a) $\alpha_s(M_Z^2)$ and (b) χ^2_{DF} from the $O(\alpha_s^2)$ fits to the jet rates as a function of renormalization scale factor f (see text).

Figs. 16(a)–30(a) for the case $f = 1$. The data are well described by $O(\alpha_s^2)$ QCD within the fit ranges. Fits were also performed *in the same ranges* for different choices of the renormalization scale f such that $10^{-4} \leq f \leq 10^2$. In each case the fitted value of $\Lambda_{\overline{\text{MS}}}$ was translated [37] to $\alpha_s(M_Z^2)$. The value of $\alpha_s(M_Z^2)$ and the corresponding χ_{DF}^2 for the fit are shown as a function of the choice of f in Figs. 31–33 for all observables.

Several features are common to the results from each observable: $\alpha_s(M_Z^2)$ depends strongly on f ; the fit quality is good over a wide range of f , typically $f \gtrsim 10^{-3}$, and there is no strong preference for a particular scale for most of the observables; at low f the fit quality deteriorates rapidly, and neither $\alpha_s(M_Z^2)$ nor its error can be interpreted meaningfully. Similar features were reported in our earlier $\alpha_s(M_Z^2)$ measurements from jet rates [5] and energy-energy correlations [6]. For the oblateness the good fit region is $f \gtrsim 10^{-1}$, which is much higher than for the other observables. For D_2 calculated in the E scheme the lowest χ_{DF}^2 is found in the region around $f \sim 10^{-4}$, which is much lower than for the other observables.

Figures 31–33 form a complete representation of the results of the fits of $O(\alpha_s^2)$ QCD to our data. It is useful, however, to quote a single value of $\alpha_s(M_Z^2)$, together with its associated uncertainties, determined from each observable. For this purpose we adopt the following procedure, similar to that adopted in our previous measurements [5,6].

For each observable an f range was defined such that $\chi_{\text{DF}}^2 < 5.0$ and $f \leq 4.0$. The former requirement excludes the low f regions where the fit quality is poor, which has been shown [38] to be due to poor convergence of the $O(\alpha_s^2)$ calculations. The latter requirement corresponds to a reasonable physical limit $\mu \leq 2\sqrt{s}$. This range is arbitrary, but does ensure that the smallest $\alpha_s(M_Z^2)$ point [see Figs. 31(a)–33(a)] is considered for all variables except B_T . The extrema of $\alpha_s(M_Z^2)$ values in this f range

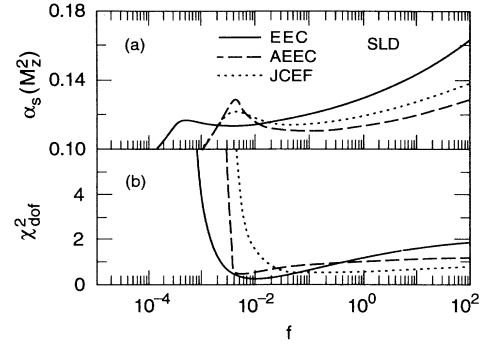


FIG. 33. (a) $\alpha_s(M_Z^2)$ and (b) χ_{DF}^2 from the $O(\alpha_s^2)$ fits to the particle correlations and angular energy flow as a function of renormalization scale factor f (see text).

were taken to define a symmetric *renormalization scale uncertainty* about their average, which we defined as the central value. The f -range, central $\alpha_s(M_Z^2)$ value, and scale uncertainty are listed in Table VIII for each observable.

For most observables the statistical error on $\alpha_s(M_Z^2)$ was defined by the change in $\alpha_s(M_Z^2)$ corresponding to an increase in χ^2 of 1.0 above the lowest value within the f range defined above [see Figs. 31(b)–33(b)]. However, for the EEC, AEEC, and JCEF, where there are strong bin-to-bin correlations, the statistical error on $\alpha_s(M_Z^2)$ was estimated by applying the same fitting procedure to ten sets of Monte Carlo events, each comprising the same number of events as the data sample, and taking the rms deviation over the ten samples. The statistical error is less than 1% of $\alpha_s(M_Z^2)$ for each observable, and is listed in Table VIII.

For each observable the experimental systematic error on $\alpha_s(M_Z^2)$ was estimated by changing the detector correction factor C_D within the systematic limits shown in

TABLE VIII. Observables used in $O(\alpha_s^2)$ QCD fits. For each the fit range, the range of the renormalization scale factor considered, central $\alpha_s(M_Z^2)$ value, statistical and experimental systematic errors, and hadronization and scale uncertainties are shown.

Observable	Fit range	f range	$\alpha_s(M_Z^2)$	Stat	Uncertainties		
					Expt syst	Had.	Scale
τ	0.06 – 0.32	$2 \times 10^{-4} - 4$	0.1245	± 0.0008	± 0.0017	± 0.0026	± 0.0201
ρ	0.04 – 0.32	$1.5 \times 10^{-3} - 4$	0.1273	± 0.0008	± 0.0020	± 0.0005	± 0.0096
B_T	0.12 – 0.32	$5.7 \times 10^{-3} - 4$	0.1272	± 0.0008	± 0.0020	± 0.0033	± 0.0220
B_W	0.06 – 0.26	$2 \times 10^{-3} - 4$	0.1196	± 0.0008	± 0.0026	± 0.0024	± 0.0072
O	0.08 – 0.32	$2 \times 10^{-1} - 4$	0.1343	± 0.0013	± 0.0015	± 0.0087	± 0.0082
C	0.24 – 0.76	$4 \times 10^{-4} - 4$	0.1233	± 0.0009	± 0.0019	± 0.0032	± 0.0186
$D_2(E)$	0.08 – 0.28	$5 \times 10^{-5} - 4$	0.1273	± 0.0006	± 0.0016	± 0.0022	± 0.0217
$D_2(E0)$	0.05 – 0.28	$1.2 \times 10^{-2} - 4$	0.1175	± 0.0007	± 0.0027	± 0.0010	± 0.0083
$D_2(P)$	0.05 – 0.22	$5.5 \times 10^{-3} - 4$	0.1207	± 0.0008	± 0.0033	± 0.0025	± 0.0053
$D_2(P0)$	0.05 – 0.28	$1.2 \times 10^{-2} - 4$	0.1190	± 0.0009	± 0.0031	± 0.0020	± 0.0057
$D_2(D)$	0.03 – 0.22	$1.7 \times 10^{-3} - 4$	0.1245	± 0.0011	± 0.0032	± 0.0007	± 0.0077
$D_2(G)$	0.12 – 0.28	$4 \times 10^{-3} - 4$	0.1191	± 0.0008	± 0.0014	± 0.0029	± 0.0043
EEC	36.0° – 154.8°	$3.5 \times 10^{-3} - 4$	0.1240	± 0.0008	± 0.0030	± 0.0031	± 0.0121
AEEC	18.0° – 68.4°	$9 \times 10^{-2} - 4$	0.1121	± 0.0012	± 0.0032	± 0.0017	± 0.0031
JCEF	100.8° – 158.4°	$5 \times 10^{-3} - 4$	0.1185	± 0.0007	± 0.0027	± 0.0008	± 0.0045

Figs. 16(c)–30(c), and by repeating the correction and fitting procedures to obtain $\Lambda_{\overline{\text{MS}}}$ and hence $\alpha_s(M_Z^2)$ values. The systematic error, calculated from the resulting spread in $\alpha_s(M_Z^2)$ values, was found to be 1–3% of $\alpha_s(M_Z^2)$ for each observable and is listed in Table VIII.

For each observable the hadronization uncertainty on $\alpha_s(M_Z^2)$ was estimated by changing the hadronization correction factor C_H within the systematic limits shown in Figs. 16(b)–30(b), and by repeating the correction and fitting procedures to obtain $\Lambda_{\overline{\text{MS}}}$ and hence $\alpha_s(M_Z^2)$ values. The hadronization uncertainty, calculated from the resulting spread in $\alpha_s(M_Z^2)$ values, was found to be 0.4–6% of $\alpha_s(M_Z^2)$ for each observable and is listed in Table VIII.

The central values of $\alpha_s(M_Z^2)$ and the errors are summarized in Table IX. For each observable the total experimental error is the sum in quadrature of the statistical and experimental systematic errors, and the total theoretical uncertainty is the sum in quadrature of the hadronization and scale uncertainties. In all cases the theoretical uncertainty, which derives mainly from the scale ambiguity, dominates. This uncertainty, which arises from uncalculated higher order terms in perturbation theory, varies from about 3% of $\alpha_s(M_Z^2)$ for the AEEC to about 17% of $\alpha_s(M_Z^2)$ for B_T . The $\alpha_s(M_Z^2)$ values from the 15 observables are consistent within these theoretical uncertainties. Since the same data were used to measure all observables, and the observables are all highly correlated, we combine these results using an unweighted average to obtain

$$\alpha_s(M_Z^2) = 0.1226 \pm 0.0026(\text{expt}) \pm 0.0109(\text{theor}),$$

where the experimental error is the sum in quadrature of the average statistical (± 0.0009) and average experimental systematic (± 0.0024) errors, corresponding to the assumption that all are completely correlated. The theoretical error is the sum in quadrature of the average hadronization (± 0.0024) and average scale (± 0.0106) uncertainties.

As a cross check we combined the results by using weighted averages. Weighting by experimental errors

TABLE IX. The $\alpha_s(M_Z^2)$ values derived from $O(\alpha_s^2)$ QCD fits.

Observable	$\alpha_s(M_Z^2)$	Expt error	Theoretical uncertainty
τ	0.1245	± 0.0019	± 0.0203
ρ	0.1273	± 0.0022	± 0.0096
B_T	0.1272	± 0.0022	± 0.0222
B_W	0.1196	± 0.0027	± 0.0076
O	0.1343	± 0.0020	± 0.0120
C	0.1233	± 0.0021	± 0.0189
$D_2(E)$	0.1273	± 0.0017	± 0.0218
$D_2(E0)$	0.1175	± 0.0028	± 0.0084
$D_2(P)$	0.1207	± 0.0034	± 0.0059
$D_2(P0)$	0.1190	± 0.0032	± 0.0060
$D_2(D)$	0.1245	± 0.0034	± 0.0077
$D_2(G)$	0.1191	± 0.0016	± 0.0052
EEC	0.1240	± 0.0031	± 0.0125
AEEC	0.1121	± 0.0034	± 0.0035
JCEF	0.1185	± 0.0028	± 0.0046

yields an average $\alpha_s(M_Z^2)$ value different from the above by +0.0009; weighting by the total errors yields an $\alpha_s(M_Z^2)$ value different by –0.0013. These differences are of the same order as the statistical error on a single $\alpha_s(M_Z^2)$ measurement and are hence negligible.

C. Measurement of $\alpha_s(M_Z^2)$ using resummed $+O(\alpha_s^2)$ calculations

We next determined $\alpha_s(M_Z^2)$ by comparing the resummed $+O(\alpha_s^2)$ calculations with the corrected data at the parton level for those observables for which the resummed $+O(\alpha_s^2)$ calculations exist, i.e., thrust (τ), heavy jet mass (ρ), total (B_T) and wide (B_W) jet broadening measures, differential two-jet rate (D_2) calculated in the D scheme, and energy-energy correlations (EEC's). We considered all four matching schemes discussed in Sec. IV, namely, $\ln R$ -, modified $\ln R$ -, R -, and modified R -matching. However, modified R -matching is not applicable to D_2 because the subleading term² G_{21} is not calculated in this case. For the EEC $\ln R$ -matching and modified $\ln R$ -matching schemes cannot be applied reliably [39] and were not used.

The fit ranges were initially chosen to be the same as for the $O(\alpha_s^2)$ fits except for the EEC, for which the fits were performed within the angular range $90^\circ \leq \chi \leq 154.8^\circ$, where the lower limit is the kinematic limit for the resummed $+O(\alpha_s^2)$ calculation. For the fit to D_2 (D scheme) we adopted a procedure [5] using the matched calculation for $0.03 \leq y_{\text{cut}} < 0.05$ and the $O(\alpha_s^2)$ calculation for $0.05 \leq y_{\text{cut}} \leq 0.33$. Fits to determine $\Lambda_{\overline{\text{MS}}}$, and hence $\alpha_s(M_Z^2)$, were performed as described in the previous section. For illustration Figs. 16(a)–19(a), 26(a), and 28(a) show the results of the resummed $+O(\alpha_s^2)$ QCD fits using the modified $\ln R$ -matching scheme with the renormalization scale factor $f = 1$. The data are well described by the QCD calculations within the fit ranges, and also beyond the fit ranges into the so-called “two-jet region” or “Sudakov region” where the resummed contributions are large [10,13]. This is discussed further at the end of this section. Figures 34–37 show (a) $\alpha_s(M_Z^2)$ and (b) the corresponding χ_{DF}^2 , derived from fits at different values of f , for the four matching schemes.

Several features should be noted from Figs. 34–37. For each matching scheme and each observable the dependence of $\alpha_s(M_Z^2)$ on f [Figs. 34(a)–37(a)] is weaker than that from the $O(\alpha_s^2)$ fits [Figs. 31(a)–33(a)]; the range of f for which the fit quality is good [Figs. 34(b)–37(b)] is in all cases smaller than the corresponding range from the $O(\alpha_s^2)$ fits [Figs. 31(b)–33(b)], and some observables, most notably B_T and B_W , do display preferences for particular scales, typically in the range $10^{-2} < f < 10$. However, using the R -matching scheme we found the fit qualities for B_T and B_W to be very poor for all scales. For a given observable, at any given f the values of $\alpha_s(M_Z^2)$ and χ_{DF}^2 are typically similar for both of the $\ln R$ -matching schemes;³ however, the results from the

²The value of G_{21} cannot be estimated until a complete calculation of G_{22} is available [39].

³In the case of the modified $\ln R$ -matching scheme the results were found to be insensitive to the values of y_{max} mentioned in Sec. IV.

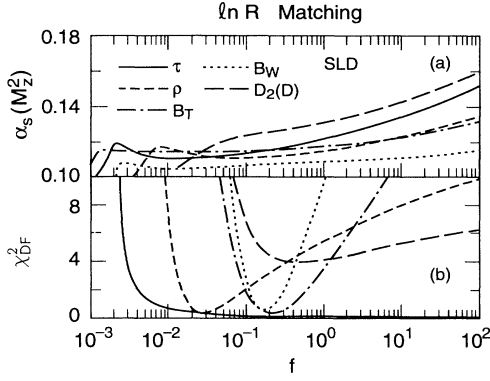


FIG. 34. (a) $\alpha_s(M_Z^2)$ and (b) χ_{DF}^2 from the resummed $+O(\alpha_s^2)$ fits with $\ln R$ matching as a function of renormalization scale factor f (see text).

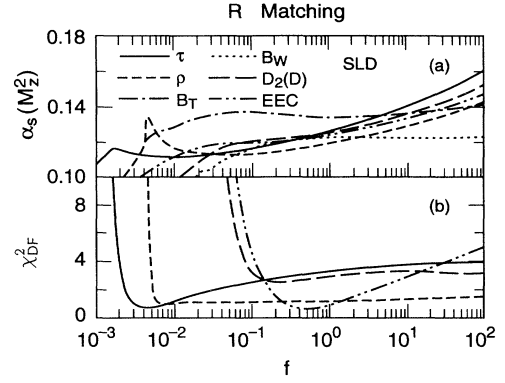


FIG. 36. (a) $\alpha_s(M_Z^2)$ and (b) χ_{DF}^2 from the resummed $+O(\alpha_s^2)$ fits with R matching as a function of renormalization scale factor f (see text). The χ_{DF}^2 values for B_T and B_W are larger than 10 for all f .

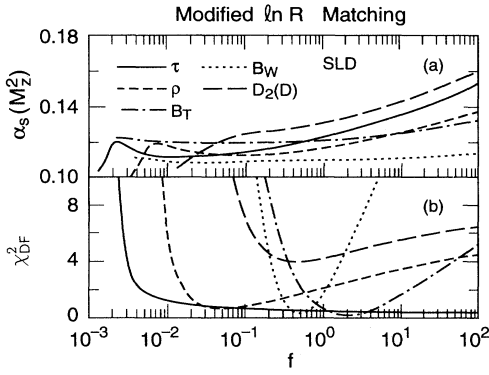


FIG. 35. (a) $\alpha_s(M_Z^2)$ and (b) χ_{DF}^2 from the resummed $+O(\alpha_s^2)$ fits with modified $\ln R$ matching as a function of renormalization scale factor f (see text).

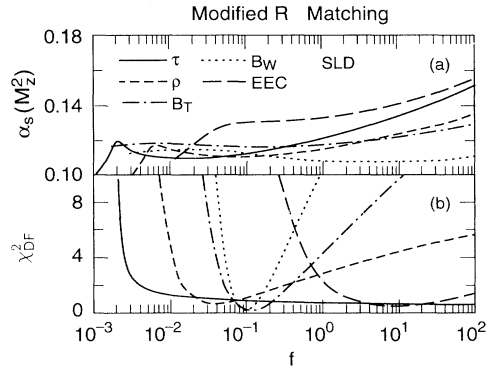


FIG. 37. (a) $\alpha_s(M_Z^2)$ and (b) χ_{DF}^2 from the resummed $+O(\alpha_s^2)$ fits with modified R matching as a function of renormalization scale factor f (see text).

TABLE X. Observables used in resummed $+O(\alpha_s^2)$ fits. For each the fit range, the range of the renormalization scale factor considered, the central $\alpha_s(M_Z^2)$ value, and scale uncertainty ($\Delta\alpha_s$) are given. Results are shown separately for each of the four matching schemes considered. Acceptable fits to the data could not be obtained for B_T and B_W with the R -matching scheme.

Observable	Fit range	$\ln R$ matching $\alpha_s(M_Z^2) \pm \Delta\alpha_s$ f range	Mod. $\ln R$ matching $\alpha_s(M_Z^2) \pm \Delta\alpha_s$ f range	R matching $\alpha_s(M_Z^2) \pm \Delta\alpha_s$ f range	Mod. R matching $\alpha_s(M_Z^2) \pm \Delta\alpha_s$ f range
τ	0.06 – 0.32	0.1196 ± 0.0089 $2.7 \times 10^{-3} - 4$	0.1203 ± 0.0089 $2.7 \times 10^{-3} - 4$	0.1226 ± 0.0110 $1.9 \times 10^{-3} - 4$	0.1187 ± 0.0091 $2.3 \times 10^{-3} - 4$
ρ	0.04 – 0.32	0.1151 ± 0.0039 $1.1 \times 10^{-2} - 4$	0.1162 ± 0.0047 $1.1 \times 10^{-2} - 4$	0.1178 ± 0.0061 $4.9 \times 10^{-3} - 4$	0.1146 ± 0.0044 $1.0 \times 10^{-2} - 4$
B_T	0.12 – 0.32	0.1175 ± 0.0030 $6.7 \times 10^{-2} - 4$	0.1211 ± 0.0015 $3.0 \times 10^{-1} - 4$		0.1177 ± 0.0017 $3.6 \times 10^{-2} - 4$
B_W	0.06 – 0.26	0.1083 ± 0.0016 $8.2 \times 10^{-2} - 4$	0.1095 ± 0.0003 $1.9 \times 10^{-1} - 4$		0.1107 ± 0.0034 $4.9 \times 10^{-2} - 4$
$D_2(D)$	0.03 – 0.22	0.1312 ± 0.0060 $1.5 \times 10^{-1} - 4$	0.1313 ± 0.0059 $1.6 \times 10^{-1} - 4$	0.1251 ± 0.0053 $7.0 \times 10^{-2} - 4$	N/A
EEC	$90.0^\circ - 154.8^\circ$	N/A	N/A	0.1239 ± 0.0049 $6.1 \times 10^{-2} - 4$	0.1336 ± 0.0028 $2.7 \times 10^{-1} - 4$

two R -matching schemes are typically systematically different both between the two schemes and with respect to the two $\ln R$ -matching schemes. Since there is *a priori* no strong reason to reject individual matching schemes from consideration, it is necessary to consider an additional theoretical uncertainty deriving from the matching ambiguity; this will be discussed below.

In order to quote a single $\alpha_s(M_Z^2)$ value, and corresponding errors, for each observable we applied the same procedure as for the $O(\alpha_s^2)$ fits to the results from each matching scheme. Table X summarizes the f ranges, central values of $\alpha_s(M_Z^2)$, and scale uncertainties. The experimental and hadronization systematic uncertainties were estimated by the methods described in Sec. VB and found to be similar to those from the $O(\alpha_s^2)$ analysis. For each observable we then took the average $\alpha_s(M_Z^2)$ value over all four matching schemes. The maximum deviation of $\alpha_s(M_Z^2)$ from the central value was defined as the matching uncertainty, and was added in quadrature with the hadronization and scale uncertainties to obtain a total theoretical uncertainty for each observable. The scale and matching uncertainties *both* derive from uncalculated higher-order perturbative contributions and are therefore correlated, although to an unknown degree. The inclusion of both contributions in the total theoretical uncertainty therefore represents a conservative, though not unreasonable, estimate of the effects of the higher-order contributions. The central $\alpha_s(M_Z^2)$ value, total experimental error, defined as the sum in quadrature of the statistical and experimental systematic errors, and the total theoretical uncertainty are listed in Table XI.

Comparing the results in Tables IX and XI it is apparent that the values of $\alpha_s(M_Z^2)$ from the resummed+ $O(\alpha_s^2)$ fits are lower than those from the $O(\alpha_s^2)$ fits by about 3% (τ), 6% (ρ), and 7% (B_T and B_W), but higher by about 4% [$D_2(D)$] and 5% (EEC). In addition, for all observables except $D_2(D)$, the theoretical uncertainty is considerably smaller for the resummed+ $O(\alpha_s^2)$ case than for the $O(\alpha_s^2)$ case, despite the extra matching uncertainty contribution to the former. For $D_2(D)$ the theoretical uncertainty is essentially the same for both $O(\alpha_s^2)$ and resummed+ $O(\alpha_s^2)$ cases, which may relate to the fact that the resummation of next-to-leading logarithms of y_{cut} to all orders of α_s is not complete [12,40]. In all cases, however, the theoretical uncertainty is larger than the experimental error.

Combining the resummed+ $O(\alpha_s^2)$ results from all six observables using an unweighted average we obtain

$$\alpha_s(M_Z^2) = 0.1192 \pm 0.0025(\text{expt}) \pm 0.0070(\text{theor}),$$

TABLE XI. The $\alpha_s(M_Z^2)$ values derived from resummed + $O(\alpha_s^2)$ QCD fits.

Observable	$\alpha_s(M_Z^2)$	Expt error	Theoretical uncertainty
τ	0.1180	± 0.0018	± 0.0115
ρ	0.1163	± 0.0020	± 0.0064
B_T	0.1160	± 0.0020	± 0.0048
B_W	0.1074	± 0.0025	± 0.0042
$D_2(D)$	0.1297	± 0.0035	± 0.0073
EEC	0.1279	± 0.0032	± 0.0069

where the total experimental error is the sum in quadrature of the average statistical (± 0.0007) and average experimental systematic (± 0.0024) errors, and the total theoretical error is the sum in quadrature of the average hadronization (± 0.0016) and average scale and matching (± 0.0065) uncertainties. As a cross check we combined the results by using weighted averages. Weighting by experimental errors yields an average $\alpha_s(M_Z^2)$ value different from the above by -0.0011 ; weighting by the total errors yields an $\alpha_s(M_Z^2)$ value different by -0.0015 . These differences are of the same order as the statistical error on a single $\alpha_s(M_Z^2)$ measurement and are hence negligible.

It is interesting to compare the resummed+ $O(\alpha_s^2)$ result with the $O(\alpha_s^2)$ result. The final value quoted in Sec. VB is the average of the $O(\alpha_s^2)$ results over all 15 observables, whereas the value quoted above is the average of the resummed+ $O(\alpha_s^2)$ results over a subset of 6 observables. For the purposes of comparison we averaged the $O(\alpha_s^2)$ results for τ , ρ , B_T , B_W , $D_2(D)$, and EEC to obtain

$$\alpha_s(M_Z^2) = 0.1242 \pm 0.0026(\text{expt}) \\ \pm 0.0132(\text{theor}).$$

For the *same set* of six observables, therefore, we find that the central $\alpha_s(M_Z^2)$ values derived from $O(\alpha_s^2)$ and resummed + $O(\alpha_s^2)$ fits in the *same range* of each observable are in agreement to within the (correlated) experimental errors, and that the theoretical uncertainty is significantly smaller when the resummed calculations are employed.

From Figs. 16(a)–19(a), 26(a), and 28(a), it is clear that the resummed+ $O(\alpha_s^2)$ calculations are more successful than the $O(\alpha_s^2)$ calculations in describing the two-jet (Sudakov) region. This implies that multiple emissions of soft gluons, which are taken into account in the resummed terms, contribute significantly to this region. Therefore, for each observable we extended the fit range into the two-jet region and extracted $\alpha_s(M_Z^2)$ as a function of the renormalization scale factor f . Requirements (1)–(3) (Sec. VB) were applied. In addition, for $D_2(D)$ we required the five-jet production rate R_5 to be less than 1%; for the EEC the upper limit of the fit range was extended to $\chi = 162^\circ$ by applying the empirical criterion $\chi_{\text{DF}}^2 < 5$. The fit ranges are listed in Table XII.

The same procedure as above was applied to define a range of renormalization scale factor f over which to calculate a central $\alpha_s(M_Z^2)$ value and scale uncertainty for each observable; the f -range, central $\alpha_s(M_Z^2)$ value, and scale uncertainty are listed in Table XII separately for fits using each of the four matching schemes. Good fits with $\chi_{\text{DF}}^2 < 5$ could not be obtained using the R -matching scheme for τ , B_T , B_W , and $D_2(D)$ for any extension of the fit range beyond that used for the $O(\alpha_s^2)$ fits. By comparing Tables X and XII it can be seen that the maximum change in $\alpha_s(M_Z^2)$ when the fit range is extended into the two-jet region is -0.0026 for τ ($\ln R$ matching), -0.0038 for ρ (R matching), -0.0009 for B_T (modified $\ln R$ matching), -0.0006 for B_W (modified $\ln R$ matching), -0.0045 for $D_2(D)$ (modified $\ln R$ matching), and -0.0006 for the EEC (R matching). These shifts

TABLE XII. Observables used in resummed+ $O(\alpha_s^2)$ fits with the fit ranges extended into the two-jet region. For each the fit range, the range of the renormalization scale factor considered, the central $\alpha_s(M_Z^2)$ value, and scale uncertainty ($\Delta\alpha_s$) are given. Results are shown separately for each of the four matching schemes considered. Acceptable fits to the data could not be obtained for τ , B_T , B_W , and $D_2(D)$ with the R -matching scheme.

Observable	Fit range	ln R matching	Mod. ln R matching	R matching	Mod. R matching
		$\alpha_s(M_Z^2) \pm \Delta\alpha_s$ f range	$\alpha_s(M_Z^2) \pm \Delta\alpha_s$ f range	$\alpha_s(M_Z^2) \pm \Delta\alpha_s$ f range	$\alpha_s(M_Z^2) \pm \Delta\alpha_s$ f range
τ	0.02 – 0.32	0.1170 \pm 0.0086 $7.0 \times 10^{-2} - 4$	0.1184 \pm 0.0075 $1.4 \times 10^{-1} - 4$		0.1191 \pm 0.0045 $6.3 \times 10^{-1} - 4$
ρ	0.02 – 0.32	0.1153 \pm 0.0071 $2.6 \times 10^{-2} - 4$	0.1146 \pm 0.0072 $3.4 \times 10^{-2} - 4$	0.1140 \pm 0.0054 $2.0 \times 10^{-1} - 4$	0.1124 \pm 0.0071 $4.0 \times 10^{-2} - 4$
B_T	0.04 – 0.32	0.1177 \pm 0.0040 $2.0 \times 10^{-1} - 4$	0.1202 \pm 0.0021 $6.7 \times 10^{-2} - 4$		0.1175 \pm 0.0023 $1.1 \times 10^{-1} - 4$
B_W	0.04 – 0.26	0.1078 \pm 0.0024 $1.4 \times 10^{-1} - 4$	0.1089 \pm 0.0014 $2.8 \times 10^{-1} - 4$		0.1106 \pm 0.0032 $5.4 \times 10^{-2} - 4$
$D_2(D)$	0.01 – 0.22	0.1269 \pm 0.0026 $1.3 \times 10^{-1} - 4$	0.1268 \pm 0.0025 $1.3 \times 10^{-1} - 4$		N/A
EEC	90.0° – 162.0°	N/A	N/A	0.1233 \pm 0.0043 $6.9 \times 10^{-2} - 4$	0.1337 \pm 0.0027 $5.0 \times 10^{-1} - 4$

are smaller than, or comparable with, the experimental errors, and are much smaller than the theoretical uncertainties.

For each observable the average $\alpha_s(M_Z^2)$ value over all four matching schemes, and the matching uncertainty, were calculated as before. The central $\alpha_s(M_Z^2)$ value, the total experimental error, and the total theoretical uncertainty, defined as before, are listed in Table XIII. Averaging over the six observables, as above, then yields

$$\alpha_s(M_Z^2) = 0.1181 \pm 0.0024(\text{expt}) \\ \pm 0.0057(\text{theor}),$$

which is in good agreement with the above average of results from the restricted fit ranges.

VI. CONCLUSIONS

We have measured the strong coupling $\alpha_s(M_Z^2)$ by analyses of 15 different observables that describe the hadronic final states of about 60 000 Z^0 decays recorded by the SLD experiment. The observables comprise six event shapes (τ , ρ , B_T , B_W , O , and C), differential two-jet rates (D_2) defined by six different jet resolution-recombination schemes (E , $E0$, P , $P0$, D , and G), energy-energy correlations (EEC) and their asymmetry (AEEC), and the jet cone energy fraction (JCEF). The

quantity JCEF has been measured for the first time. Our measured distributions of these observables are reproduced by the JETSET and HERWIG Monte Carlo simulations of hadronic Z^0 decays. The coupling was determined by fitting perturbative QCD calculations to the data corrected to the parton level. Perturbative QCD calculations complete to $O(\alpha_s^2)$ were used for all 15 observables. In addition, recently performed resummed calculations were matched to the $O(\alpha_s^2)$ calculations using four matching schemes and applied to the six observables for which the resummed calculations are available.

We find that the $O(\alpha_s^2)$ calculations are able to describe the data in the hard three-jet region of all 15 observables for a wide range of the QCD renormalization scale factor f . The fitted $\alpha_s(M_Z^2)$ value depends strongly both on the choice of f , which limits the precision of the $\alpha_s(M_Z^2)$ measurement from each observable, and on the choice of observable. The AEEC shows the smallest renormalization scale uncertainty of about 3%, which is just larger than the experimental error. The $\alpha_s(M_Z^2)$ values determined from jet rates and energy-energy correlations are consistent with our previous measurements [5,6] within experimental errors. The $\alpha_s(M_Z^2)$ values from the various observables are consistent with each other only within the scale uncertainties. The large-scale uncertainties and systematically different $\alpha_s(M_Z^2)$ values determined from different observables imply that the uncalculated $O(\alpha_s^3)$ perturbative QCD contributions are significant and cannot be ignored if $\alpha_s(M_Z^2)$ is to be determined with a precision of better than 10%.

The resummed+ $O(\alpha_s^2)$ calculations yield a reduced renormalization scale dependence of $\alpha_s(M_Z^2)$, and fit a wider kinematic region, including the two-jet or Sudakov region, and give similar fitted values of $\alpha_s(M_Z^2)$ to the $O(\alpha_s^2)$ case. However, the different matching schemes give different $\alpha_s(M_Z^2)$ values, which reflects a residual uncertainty in the inclusion of terms in the resummed+ $O(\alpha_s^2)$ calculations. For all observables except $D_2(D)$ the theoretical uncertainty is smaller than in the $O(\alpha_s^2)$ case, but still dominates the uncertainty in

TABLE XIII. The $\alpha_s(M_Z^2)$ values derived from resummed+ $O(\alpha_s^2)$ QCD fits with the fit ranges extended into the two-jet region.

Observable	$\alpha_s(M_Z^2)$	Expt error	Theoretical uncertainty
τ	0.1159	± 0.0017	± 0.0090
ρ	0.1144	± 0.0019	± 0.0074
B_T	0.1157	± 0.0020	± 0.0053
B_W	0.1070	± 0.0025	± 0.0041
$D_2(D)$	0.1274	± 0.0034	± 0.0027
EEC	0.1285	± 0.0032	± 0.0068

the measurement of $\alpha_s(M_Z^2)$. Again, the $\alpha_s(M_Z^2)$ values derived from jet rates and energy-energy correlations are consistent with our previous measurements [5,6] within experimental errors, and the values determined from the six observables are consistent within theoretical uncertainties.

Figure 38 summarizes the measured $\alpha_s(M_Z^2)$ values from all 15 observables using $O(\alpha_s^2)$ calculations, and from the six observables using resummed+ $O(\alpha_s^2)$ calculations in the extended kinematic region. Since the same data were used to measure all observables, and the observables are highly correlated, we combined the results by taking unweighted averages of the $\alpha_s(M_Z^2)$ values and experimental and theoretical errors, obtaining

$$\begin{aligned}\alpha_s(M_Z^2) &= 0.1226 \pm 0.0026(\text{expt}) \\ &\quad \pm 0.0109(\text{theor}) O(\alpha_s^2), \\ \alpha_s(M_Z^2) &= 0.1181 \pm 0.0024(\text{expt}) \\ &\quad \pm 0.0057(\text{theor}) \text{ resummed} + O(\alpha_s^2),\end{aligned}$$

where in both cases the theoretical uncertainty is dominated by the lack of knowledge of higher-order terms in the QCD calculations. Our estimate of the theoretical uncertainty is larger than that quoted by some of the LEP experiments because we have considered more observables and wider variations of the renormalization scale, and have taken unweighted averages. These average values are shown in Fig. 38; they are consistent with measurements from other e^+e^- experiments at the Z^0 resonance [27,30,31,39,41] and from lower energy e^+e^- and deep-inelastic-scattering experiments [42].

One expects *a priori* the $\alpha_s(M_Z^2)$ value determined from a resummed+ $O(\alpha_s^2)$ fit to be more reliable than that from an $O(\alpha_s^2)$ fit. However, the former is only available for 6 of the 15 observables. In order to quote a final result, therefore, we took the unweighted average of the $\alpha_s(M_Z^2)$ values and uncertainties over the combined set of six resummed+ $O(\alpha_s^2)$ results and nine $O(\alpha_s^2)$ results for which there is no corresponding resummed+ $O(\alpha_s^2)$ result. This yields a final average of

$$\alpha_s(M_Z^2) = 0.1200 \pm 0.0025(\text{expt}) \pm 0.0078(\text{theor}),$$

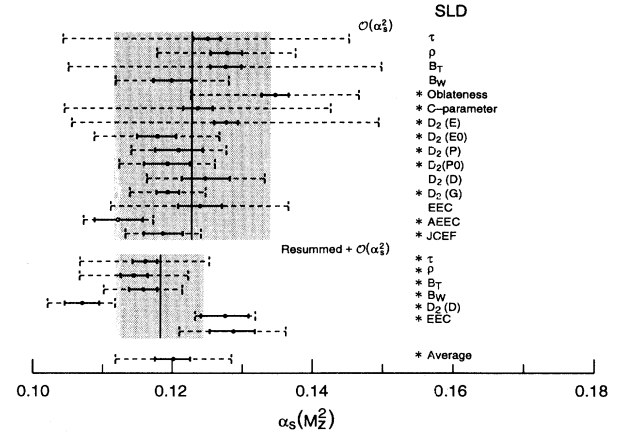


FIG. 38. Compilation of final values of $\alpha_s(M_Z^2)$. For each observable the solid bar denotes the experimental error, while the dashed bar shows the total uncertainty comprising the experimental error and theoretical uncertainty in quadrature. Shown separately for the $O(\alpha_s^2)$ results and resummed+ $O(\alpha_s^2)$ results are a vertical line and a shaded region representing the average $\alpha_s(M_Z^2)$ value and uncertainty, respectively, in each case. Also shown is the final average of six resummed+ $O(\alpha_s^2)$ and nine $O(\alpha_s^2)$ results indicated by stars.

also shown in Fig. 38, corresponding to $\Lambda_{\overline{\text{MS}}} = 253_{-96}^{+130}$ MeV.

ACKNOWLEDGMENTS

We thank the personnel of the SLAC accelerator department and the technical staffs of our collaborating institutions for their efforts which resulted in the successful operation of the SLC and the SLD. We also thank S. J. Brodsky, S. D. Ellis, K. Kato, P. Nason, and D. Ward for helpful comments and suggestions relating to this analysis.

- [1] SLD Collaboration, K. Abe *et al.*, Phys. Rev. Lett. **73**, 25 (1994); LEP Collaborations and LEP Electroweak Working Group, CERN Report No. CERN-PPE-93-157, 1993 (unpublished).
- [2] H. Fritzsch, M. Gell-Mann, and H. Leutwyler, Phys. Lett. **47B**, 365 (1973); D. J. Gross and F. Wilczek, Phys. Rev. Lett. **30**, 1343 (1973); H. D. Politzer, *ibid.* **30**, 1346 (1973).
- [3] W. A. Bardeen *et al.*, Phys. Rev. D **18**, 3998 (1978).
- [4] S. J. Brodsky and H. J. Lu, SLAC Report No. SLAC-PUB-6481, 1994 (unpublished).
- [5] SLD Collaboration, K. Abe *et al.*, Phys. Rev. Lett. **71**, 2528 (1993).
- [6] SLD Collaboration, K. Abe *et al.*, Phys. Rev. D **50**, 5580 (1994).
- [7] Z. Kunszt, P. Nason, G. Marchesini, and B. R. Webber, in *Z Physics at LEP I*, Proceedings of the Work-

- shop, Geneva, Switzerland, 1989, edited by G. Altarelli, R. Kleiss, and C. Verzegnassi [CERN Report No. 89-08, Geneva, 1989 (unpublished)].
- [8] S. Bethke *et al.*, Nucl. Phys. **B370**, 310 (1992).
- [9] C. L. Basham *et al.*, Phys. Rev. Lett. **41**, 1585 (1978); Phys. Rev. D **17**, 2298 (1978); **19**, 2018 (1979).
- [10] S. Catani, G. Turnock, B. R. Webber, and L. Trentadue, Phys. Lett. B **263**, 491 (1991).
- [11] S. Catani, G. Turnock, and B. R. Webber, Phys. Lett. B **272**, 368 (1991).
- [12] S. Catani, Yu. L. Dokshitzer, M. Olsson, G. Turnock, and B. R. Webber, Phys. Lett. B **269**, 432 (1991).
- [13] S. Catani, G. Turnock, and B. R. Webber, CERN Report No. CERN-TH-6570/92, 1992 (unpublished).
- [14] G. Turnock, Institute Report No. Cavendish-HEP-92/3 (1992) (unpublished).
- [15] S. Catani, L. Trentadue, G. Turnock, and B. R. Webber,

- Nucl. Phys. **B407**, 3 (1993).
- [16] SLD Design Report, SLAC Report No. 273, 1984 (unpublished).
- [17] C. J. S. Damerell *et al.*, Nucl. Instrum. Methods A **288**, 288 (1990).
- [18] D. Axen *et al.*, Nucl. Instrum. Methods A **328**, 472 (1993).
- [19] A. C. Benvenuti *et al.*, Nucl. Instrum. Methods A **290**, 353 (1990).
- [20] S. Brandt *et al.*, Phys. Lett. **12**, 57 (1964); E. Farhi, Phys. Rev. Lett. **39**, 1587 (1977).
- [21] T. Sjöstrand and M. Bengtsson, Comput. Phys. Commun. **43**, 367 (1987).
- [22] G. Marchesini *et al.*, Comput. Phys. Commun. **67**, 465 (1992).
- [23] Mark J Collaboration, D. P. Barber *et al.*, Phys. Rev. Lett. **43**, 830 (1979); Phys. Lett. **89B**, 139 (1979).
- [24] G. Parisi, Phys. Lett. **74B**, 65 (1978); J. F. Donoghue, F. E. Low, and S. Y. Pi, Phys. Rev. D **20**, 2759 (1979).
- [25] L. Clavelli, Phys. Lett. **85B**, 111 (1979).
- [26] S. Catani, G. Turnock, and B. R. Webber, Phys. Lett. B **295**, 269 (1992).
- [27] Mark II Collaboration, S. Komamiya *et al.*, Phys. Rev. Lett. **64**, 987 (1990).
- [28] JADE Collaboration, W. Bartel *et al.*, Z. Phys. C **33**, 23 (1986).
- [29] Y. Ohnishi and H. Masuda, SLAC Report No. SLAC-PUB-6560, 1994 (unpublished).
- [30] DELPHI Collaboration, P. Abreu *et al.*, Z. Phys. C **59**, 21 (1993).
- [31] ALEPH Collaboration, D. Decamp *et al.*, Phys. Lett. B **284**, 163 (1992).
- [32] B. R. Webber, in *QCD—20 Years Later*, Proceedings of the Workshop, Aachen, Germany, 1992, edited by P. Zerwas and H. A. Kastrup (World Scientific, Singapore, 1993), p. 73.
- [33] P. N. Burrows, Z. Phys. C **41**, 375 (1988); OPAL Collaboration, M. Z. Akrawy *et al.*, *ibid.* **47**, 505 (1990).
- [34] CLEO Collaboration, R. Giles *et al.*, Phys. Rev. D **30**, 2279 (1984); ARGUS Collaboration, H. Albrecht *et al.*, Z. Phys. C **54**, 13 (1992); **58**, 191 (1993).
- [35] V. Blobel, in *Proceedings of 8th CERN School of Computing*, Aiguablava, Spain, 1989, edited by C. Verkerk (CERN Report No. 85-09, Geneva, Switzerland, 1985).
- [36] T. Sjöstrand, CERN Report No. CERN-TH-6488-92, 1992 (unpublished).
- [37] Particle Data Group, K. Hikasa *et al.*, Phys. Rev. D **45**, S1 (1992), p. III.54.
- [38] P. N. Burrows and H. Masuda, Z. Phys. C **63**, 235 (1994).
- [39] OPAL Collaboration, P. D. Acton *et al.*, Z. Phys. C **59**, 1 (1993).
- [40] C. N. Lovett-Turner, Phys. Lett. B **329**, 361 (1994).
- [41] L3 Collaboration, O. Adriani *et al.*, Phys. Lett. B **284**, 471 (1992).
- [42] S. Bethke, in *Proceedings of the XXVIth International Conference on High Energy Physics*, Dallas, Texas, 1992, edited by J. Sanford, AIP Conf. Proc. No. 272 (AIP, New York, 1993), p. 81.

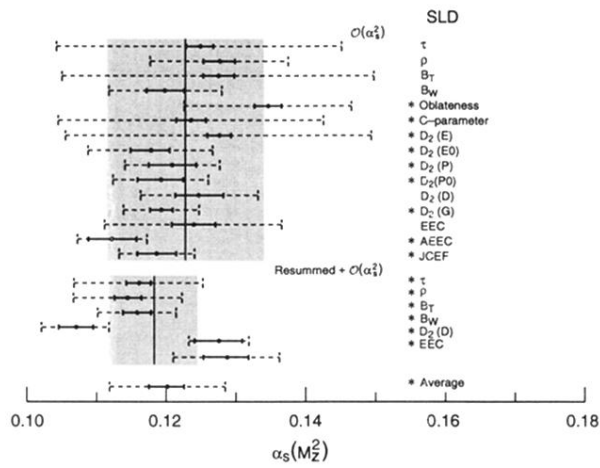


FIG. 38. Compilation of final values of $\alpha_s(M_Z^2)$. For each observable the solid bar denotes the experimental error, while the dashed bar shows the total uncertainty comprising the experimental error and theoretical uncertainty in quadrature. Shown separately for the $O(\alpha_s^2)$ results and resummed+ $O(\alpha_s^2)$ results are a vertical line and a shaded region representing the average $\alpha_s(M_Z^2)$ value and uncertainty, respectively, in each case. Also shown is the final average of six resummed+ $O(\alpha_s^2)$ and nine $O(\alpha_s^2)$ results indicated by stars.